Development of Breakdown Test Setup for Liquid and Solid Insulation Materials for High Voltage Cable Accessories

Master's thesis in Electric Power Engineering

SILVIYA JOY
SONA SUSAN DANIEL

DEPARTMENT OF ELECTRICAL ENGINEERING

CHALMERS UNIVERSITY OF TECHNOLOGY
Gothenburg, Sweden 2026
www.chalmers.se

Master's thesis 2026

Development of Breakdown Test Setup for Liquid and Solid Insulation Materials for High Voltage Cable Accessories

SILVIYA JOY
SONA SUSAN DANIEL

Department of Electrical Engineering
Division of Electric Power Engineering
Chalmers University of Technology
Gothenburg, Sweden 2026

Development of Breakdown Test Setup for Liquid and Solid Insulation Materials for High Voltage Cable Accessories
SILVIYA JOY
SONA SUSAN DANIEL

Supervisor: Susanne Nilsson, Head of R&D, Technology Basics- HV Cable Accessories Technology at NKT Accessories, Alingsås
Sajjad Jafari, HV Specialist Accessories Technology at NKT Accessories, Alingsås
Rashid Hussain, Senior Specialist HV Accessories at NKT Accessories, Alingsås
Examiner: Yuriy Serdyuk, Professor,Department of Electrical Engineering

Master's Thesis 2026
Department of Electrical Engineering
Division of Electric Power Engineering
Chalmers University of Technology
SE-412 96 Gothenburg
Telephone +46 31 772 1000

Cover: NKT high-voltage power cable

Typeset in LaTeX
Gothenburg, Sweden 2026

Development of Breakdown Test Setup for Liquid and Solid Insulation Materials for High Voltage Cable Accessories
SILVIYA JOY
SONA SUSAN DANIEL
Department of Electrical Engineering
Chalmers University of Technology

Abstract

High-voltage cable accessories rely on interfaces between solid polymeric insulation and insulating liquids, also referred to as lubricants, to accommodate dimensional tolerances during installation and reduce local electric field stress. These interfaces are often the weakest point in cable joint, yet standardized breakdown test methods that account for both material types remain limited. This thesis addresses this research gap by developing and improvising experimental breakdown test setups for the solid insulation materials which is unfilled EPDM and filled EPDM (also called FGM), and liquid insulations silicone oil and silicone grease, under both AC and DC voltage.

The work combines physical breakdown testing with COMSOL simulations of the electric field distribution at stress points (triple point or other stress regions) along with Weibull analysis to characterize breakdown strength of insulation materials across various electrode geometries. Moulded design was iteratively refined to reduce air cavities and control sample gap distance and a dedicated liquid test cell was developed to enable controlled and reproducible breakdown testing of high viscous lubricants.

This report will give an insight into the motivation behind testing both insulation materials, the underlying physics of electric field and breakdown behaviour and the experimental setups developed over the course of the thesis. The resulting findings on how test geometry and material properties influence breakdown performance were investigated and explained in the results chapter.

Keywords: EPDM, FGM, silicone oil, silicone grease, electric field distribution, breakdown strength, COMSOL Multiphysics, Weibull analysis, HVDC cable accessories, electrode geometry.

Acknowledgements

We would like to express our sincere gratitude to everyone who guided us throughout the course of this thesis.

First, we thank our examiner, Professor Yuriy Serdyuk at the Division of Electric Power Engineering, Chalmers University of Technology, for his guidance, valuable feedback, and continued engagement with our work throughout the project. We would also like to thank Xiangdong Xu, Researcher, and Thomas Hammarström, Associate Professor, Department of Electrical Engineering, at Chalmers University of Technology, for their help and technical input during the course of this project.

At NKT, we were fortunate to have Sajjad Jafari, HV Specialist, Accessories Technology, and Rashid Hussain, Senior Specialist, HV Accessories, as supervisors from the very start. Sajjad's steady involvement and coordination kept the project moving through all it's phases; and Rashid's close reading of our work, especially the simulation and technical sections, sharpened both our understanding and how we chose to present them. We are grateful for their patience with our early mistakes and for treating our questions (however basic) with genuine seriousness. We would also like to thank Susanne Nilsson, Head of R&D, Technology Basics-HV Cable Accessories Technology, for her support throughout this project.

We would also like to thank the lab and workshop staff at NKT's Alingsås facility, who helped us troubleshoot equipment, source materials, and rebuild our test setups more times than any of us would care to count, and our colleagues there, who made the long days in the lab far more enjoyable than they had any right to be.

Finally, we thank our families and friends for their unwavering support and encouragement throughout this thesis and our studies at Chalmers.

Silviya Joy and Sona Susan Daniel, Gothenburg, August 2026

List of Acronyms

Below is the list of acronyms that have been used throughout this thesis listed in alphabetical order:

AC	Alternating Current
BDV	Breakdown Voltage
COMSOL	COMSOL Multiphysics (simulation software)
DC	Direct Current
EPDM	Ethylene Propylene Diene Monomer
FEM	Finite Element Method
FGM	Field-Grading Material
HVDC	High Voltage Direct Current
HVAC	High Voltage Alternating Current
IEC	International Electrotechnical Commission
PMMA	Polymethyl Methacrylate

Contents

List of Figures

List of Tables

1

Introduction

Cable accessories - joints and terminations - are the point where a power cable is most likely to fail, since they interrupt the otherwise continuous, factory-controlled insulation of the cable itself and introduce interfaces that have to be built up correctly on site. As transmission distances grow, particularly for connecting offshore wind and other remote renewable sources to the grid, HVDC transmission is increasingly preferred over HVAC because of its lower losses over long distances. This shift sets a demand on cable accessory manufacturers: materials and designs that have records under AC stress cannot be assumed to perform the same way under DC, where the field distribution is governed by conductivity rather than permittivity and can shift over time as the material heats and space charge accumulates.

NKT, which manufactures HVDC and HVAC cable joints and terminations at its Alingsås facility among others, has been building up in-house laboratory capability to characterise the rubber and liquid materials used in these accessories under both AC and DC stress. This thesis develops and verifies breakdown test cells for this purpose, using unfilled EPDM and filled EPDM (FGM) as the solid materials under test, and extends the scope to include a systematic study of the liquid insulation and lubricant materials silicone oil and silicone grease, with a lower-viscosity silicone oil additionally used as the surrounding test medium during solid-sample testing, to prevent surface flashover, and, in a real accessory, at the rubber-to-cable interface.

1.1 Thesis work motivation

The aim of this project is to develop and verify a breakdown testing setup that covers both solid and liquid insulation materials used in cable accessories. It helps build a theoretical and experimental basis for comparing results across different electrode geometries and surrounding media.

For the solid materials: unfilled EPDM and filled EPDM (FGM), this means designing plate (both electrodes exposed), half-mould (top electrode embedded) and full-mould (both electrodes embedded) sample electrode configurations that reduce known sources of variability in breakdown testing, in particular air cavities introduced during moulding and uncontrolled triple-point geometry at the sample edge. For the liquid materials, silicone oil and silicone grease, this means characterising their own dielectric behaviour and breakdown strength rather than treating them only as a passive surrounding medium chosen to prevent flashover and provide lubrication.

Short-time breakdown testing in this project uses two different sample setups. In first setup, plate shaped samples are surrounded by an insulating liquid to suppress surface flashover. In second setup, a moulded-electrode sample with no surrounding liquid is used , which removes the uncontrolled triple point at the sample edge at the cost of a more demanding sample preparation process while requiring more material.

1.2 Scope and structure of the thesis

This thesis is organised around the two material categories introduced above. On the solid side, AC and DC breakdown testing is carried out on unfilled EPDM and filled EPDM (FGM) using three sample electrode configurations: plate, half-mould, and full-mould to isolate the effect of electrode geometry and triple-point condition from the intrinsic strength of the material itself. On the liquid side, silicone oil and silicone grease are characterised as dielectric materials in their own right through breakdown strength testing, while a separate, lower-viscosity silicone oil is used as the surrounding medium in the solid-sample tests, so that its influence on the solid-sample results can be separated from the solid material's own behaviour.

Chapter 2 develops the theoretical framework needed to interpret these results to see the effect of electrode configuration on field distribution (uniform or non-uniform field distribution) and the breakdown mechanisms expected in each material under each condition. Later chapters describe the test-cell and sample designs used, present the AC and DC breakdown results for both material categories, and compare them using Weibull statistics to separate genuine differences in material strength from differences introduced by electrode geometry or sample preparation.

2

Theoretical Background and Methodology

2.1 Field Theory

The starting point for any insulation design problem is the electrostatic or, under DC, the quasi-electrostatic conduction field set up between the electrodes. In a charge-free, source-free dielectric region the field obeys Laplace's equation,

$$\nabla^2 V = 0, \tag{2.1}$$

where V is the scalar electric potential and the local field is $\mathbf{E} = -\nabla V$.

Under DC, once the initial capacitive transient has decayed, the governing equation follows from the conservation of current, $\nabla \cdot \mathbf{J} = 0$ with $\mathbf{J} = \sigma \mathbf{E}$, which for a region of uniform conductivity reduces to the same Laplace form. Solving this equation for the given electrode geometry and boundary condition gives the field distribution $E(x)$ between the electrodes, from which the maximum local field E_{max} the quantity that governs breakdown can be extracted.

For design purposes, it is convenient to compare E_{max} with the average field, $E_{\text{mean}} = V/d$, where V is the applied voltage and d the electrode gap. The ratio of the two defines the Schwaiger factor η [1]:

$$\eta = \frac{E_{\text{mean}}}{E_{\text{max}}} = \frac{V}{d\,E_{\text{max}}}, \qquad 0 < \eta \leq 1. \tag{2.2}$$

$\eta = 1$ describes a perfectly uniform (parallel-plane)field; as the electrode geometry becomes sharper or more asymmetric, η falls, indicating that the field is increasingly concentrated at one point. If breakdown were governed purely by E_{max} reaching the material's intrinsic breakdown strength E_b, the breakdown voltage would follow directly as

$$V_b = E_{\text{max}}\,d\,\eta = E_b\,d\,\eta. \tag{2.3}$$

For non-uniform fields ($\eta < 1$), partial discharges and space-charge accumulation at lower voltages progressively change the field distribution, causing the measured breakdown voltage to deviate from the theoretical prediction well before $\eta \to 0$ [1].

2.1.1 Field distributions relevant to cable and test-cell geometry

Two closed-form field solutions recur throughout cable-accessory and breakdown-cell design.

2.1.1.0.1 Coaxial cylinders. For a cable or a cylindrical test cell with inner conductor radius r_1 and outer (insulation) radius r_2, the field varies radially as

$$E(x) = \frac{V}{x \ln(r_2/r_1)}, \tag{2.4}$$

which is maximum at the inner conductor surface, $E_{\max} = V/\big(r_1 \ln(r_2/r_1)\big)$. This is the field distribution present along the length of a cable and is the reason graded, multi-layer insulation is used to relieve the stress concentration at the conductor surface.

2.1.1.0.2 Sphere-to-plane. For a sphere of radius R at gap d above a plane, valid for $d \ll R$ (near-uniform field, $\eta \to 1$),

$$E_{\max} = 0.9\,\frac{V}{d} \cdot \frac{R + d}{R}. \tag{2.5}$$

This geometry or its close relative, a rounded ("mushroom") high-voltage electrode over a plate is the standard choice when the intrinsic dielectric strength of a material, rather than its behaviour at a sharp defect, is the property under investigation, because it keeps η close to unity and avoids introducing an artificial field concentration that the material itself does not experience in service.

2.1.2 Field uniformity in cable accessories and electrode configurations

In the cable body itself, the field is close to purely radial and well approximated by the coaxial-cylinder solution above, a field that varies only with radial distance and remains uniform along the cable's length. The moment the cable's outer semiconductive screen is cut back to build a joint or termination, however, that symmetry is broken, equipotential lines that were evenly spaced along the cable crowd together at the cut edge, and a strong tangential field component appears exactly where the screen ends. This screen-cut point is the single most field-concentrated location in a cable accessory and it is the physical reason FGM and other stress-control methods exist it is not a generic design preference but a direct response to a locally non-uniform field created by the geometry of the joint itself [2].

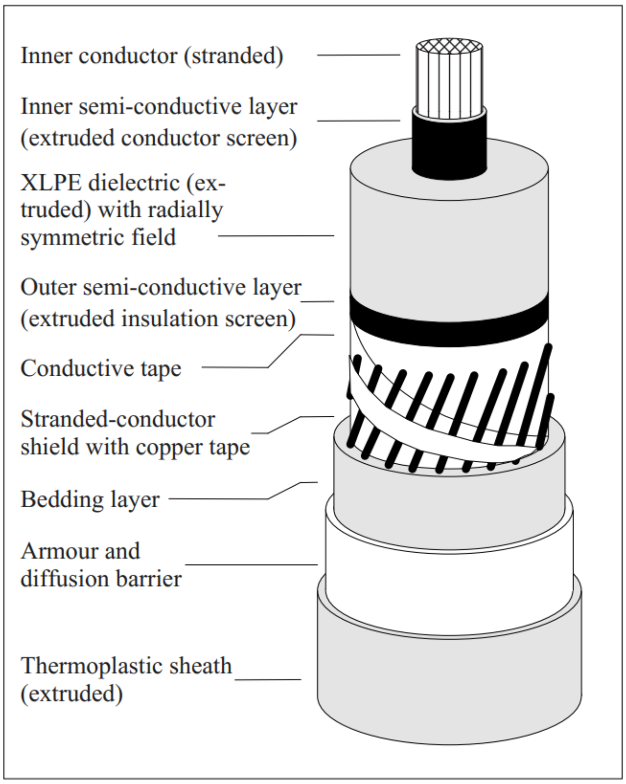

Figure 2.1: Single-conductor XLPE High Voltage Cable - Schematic Representation. [3]

Figure 2.1 shows the schematic of a single-core XLPE cable, consisting of a stranded conductor, inner semi-conductive conductor screen, XLPE insulation, and an outer semi-conductive insulation screen, together with the metallic screen and outer protective layers. In the cable body, the coaxial geometry produces a radially symmetric electric field distribution. During joint or termination installation, the insulation screen must be cut back, creating a discontinuity in the cable geometry. This loss of radial symmetry leads to electric field concentration at the screen edge, making field grading necessary to control electrical stress.

Based on the field efficiency factor η defined above (or its inverse, the field factor $f = 1/\eta$ used by [5]), three types of fields are described below:

- **Homogeneous (uniform) field** - η close to 1 (f close to 1). Realised in practice by large-radius sphere-to-sphere or plane-to-plane electrodes at small gap, such as the IEC 60052 standard sphere gap. Breakdown here is governed by the intrinsic strength of the material, since there is no significant local field concentration to bias the result.

- **Quasi-uniform field** - a moderate departure from uniformity, typically produced by sphere-to-plane or rounded ("mushroom") electrode-to-plane geometries. This is the regime the plate-sample AC/DC tests in this project are designed to sit in: enough curvature to define a repeatable maximum-stress point, but not so sharp that the result is dominated by electrode geometry rather than material strength.

- **Non-uniform (divergent) field** - η well below 1 (f large), produced by needle-to-plane, rod-to-plane, or any sharp-edged/embedded electrode. [5] $f \approx 10$ It is a practical numerical boundary below which a field can reasonably be called uniform for breakdown-mechanism purposes. Fields at a triple point or an unintended manufacturing defect fall into this category regardless of the nominal test-cell geometry, the direct link to the triple-point breakdown discussed in 2.3.1.

Sphere-sphere and sphere-plane (or sphere-cylinder) electrodes are the standard choice for homogeneous/ quasi-uniform field testing, and form the basis of the IEC 60243-1 AC test geometry used in this project. Mushroom (rounded high-voltage electrode over a flat plate) geometries push this further toward uniformity while keeping a single, repeatable maximum-stress location, which is why this shape is used for the AC/DC plate-sample tests here. Needle-to-plane and rod-to-plane electrodes deliberately create a strongly divergent field, and are the standard choice when the object of study is streamer propagation or partial-discharge behaviour itself (2.4.4), rather than its intrinsic strength under a uniform field.
This distinction matters because breakdown testing under a divergent field still measures a form of intrinsic dielectric strength, where non-uniform stress is intentionally introduced by varying one parameter. Such conditions can occur in service due to factors such as contaminants or uneven semiconductive layers and should not be confused with an unintended loss of field uniformity caused by defects such as cavities or uncontrolled triple points, which this project's near-uniform test geometries are specifically designed to avoid.

2.2 Factors Affecting the Electric Field

The field distribution described in 2.1 depends on four factors. These are explained in the next chapters and if any one of them changes, $E_{\max}$ shifts, hence the breakdown voltage shifts even when the applied voltage and nominal gap are held fixed.

2.2.1 Electrode geometry

Sharp electrodes having smaller radii of curvature, and asymmetric gaps concentrate the field at the sharper electrode, lowering η and, for a fixed applied voltage, increasing $E_{\max}$ well above the nominal field V/d. Hence the choice between a sphere/mushroom electrode (near-uniform) and a needle or embedded electrode (strongly divergent) is a design decision in its own right rather than merely a practical convenience, as it determines which breakdown mechanism is being tested (2.3.1, 2.4.4).

2.2.2 Material properties: relative permittivity versus electrical conductivity

Which material property controls the field split across a series dielectric stack depends on the applied voltage waveform and, more precisely, on the electrical time constant of each material relative to the timescale of the applied voltage. This is most easily introduced for two arbitrary dielectrics stacked in series between parallel-plate electrodes, as shown in figure 2.2, with different electrical properties.

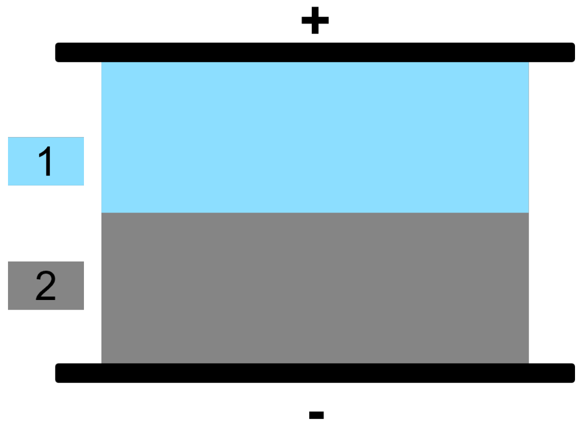

Figure 2.2: Two-layer series dielectric stack with different electrical properties placed between parallel-plate electrodes

The total current density in a dielectric under an applied field E has a conduction component and a displacement component. In the time domain,

$$J = \sigma E + \varepsilon_r \varepsilon_0 \frac{\partial E}{\partial t}, \tag{2.6}$$

where σ is the electrical conductivity, ε_r is the relative permittivity, and ε_0 is the permittivity of free space. For a sinusoidal field at angular frequency ω, this is more conveniently written in the frequency domain as

$$J = \sigma E + j\omega \varepsilon_0 \varepsilon_r E, \tag{2.7}$$

where the first term is the conduction (loss) current and the second is the displacement (capacitive) current, now 90° out of phase with it. The ratio of the two terms is $\sigma/(\omega\varepsilon_r\varepsilon_0)$. When this ratio is small ($\omega\varepsilon_r\varepsilon_0 \gg \sigma$, the low-loss case), the displacement current dominates and the field distributes itself according to relative permittivity, ε_r. Because relative permittivity is essentially temperature-independent, the field pattern set up at the instant voltage is applied then persists. This is the case for high-resistive materials such as the unfilled EPDM used in this work, and for the test liquids, whose electrical conductivity is low and only weakly field-dependent.

When $\sigma/(\omega\varepsilon_r\varepsilon_0)$ is instead large, the conduction current dominates and the field distributes itself according to electrical conductivity, σ. Under DC excitation, once the initial capacitive transient has decayed, conductivity dominates the field distribution as there is no displacement current in steady state. Under AC excitation, the same conductivity-controlled behaviour can still occur if σ is large enough relative to $\omega\varepsilon_r\varepsilon_0$ which is exactly the situation for FGM at higher fields, where its electrical conductivity increases sharply and nonlinearly once the switching field is exceeded (2.3.4). This means the statement that "AC fields are permittivity-controlled and DC fields are conductivity-controlled" only strictly holds for a material with low, weakly field-dependent conductivity. For FGM the same distinction depends on the applied field level. At sufficiently high field the distribution becomes resistive (conductivity-controlled) even under AC excitation.

For the simple two-layer stack of Figure 2.2, these two limits give two corresponding relations as how the field splits between the layers. In the low-loss, permittivity-controlled limit (displacement current continuous across the interface, $D_1 = D_2$),

$$\frac{E_1}{E_2} = \frac{\varepsilon_{r2}}{\varepsilon_{r1}}, \tag{2.8}$$

so each layer carries a field stress inversely proportional to its relative permittivity. In the conductivity-controlled DC steady state (conduction current continuous across the interface, $J_1 = J_2$),

$$\frac{E_1}{E_2} = \frac{\sigma_2}{\sigma_1}, \tag{2.9}$$

so each layer instead carries a field stress inversely proportional to its electrical conductivity.

Equivalently, the choice between Equations 2.8 and 2.9 can be expressed by comparing the material's own dielectric relaxation time constant, $\tau = \varepsilon_r\varepsilon_0/\sigma$, to the electrical time constant of the applied voltage the period of the waveform $(1/\omega)$ for AC, or the ramp timescale for DC. Electrical conductivity in polymeric and liquid dielectrics is also strongly temperature-dependent, so under DC the field pattern is not fixed even when the initial transient has decayed, it can continue to migrate as thermal gradients develop and as space charge accumulates at interfaces and within the bulk material.

This distinction is captured formally by the complex relative permittivity,

$$\varepsilon_r^* = \varepsilon_r' - j\,\varepsilon_r'', \tag{2.10}$$

where the real part ε_r' represents how strongly the material gets electrically polarized, and the imaginary part ε_r'' represents the dielectric losses, which consist of both polarization losses and conduction losses. A material with negligible ε_r'' behaves capacitively, as assumed for EPDM and the test liquids above; a material with significant, field-dependent ε_r'' - such as FGM above its switching threshold - behaves increasingly resistively.

Figure 2.3 illustrates the practical consequence of Equations 2.8 and 2.9 for a representative case relevant to this project: the two layers have a similar relative permittivity, $\varepsilon_{r1} \approx \varepsilon_{r2}$, while their electrical conductivities differ by one to two orders of magnitude, $\sigma_2/\sigma_1 \approx$ 10-100. Under AC excitation the near-equal permittivities keep the field split close to even between the two layers. Under DC excitation, however, Equation 2.9 pushes almost all of the field into the layer with the lower conductivity, even though the two layers looked electrically similar under AC.

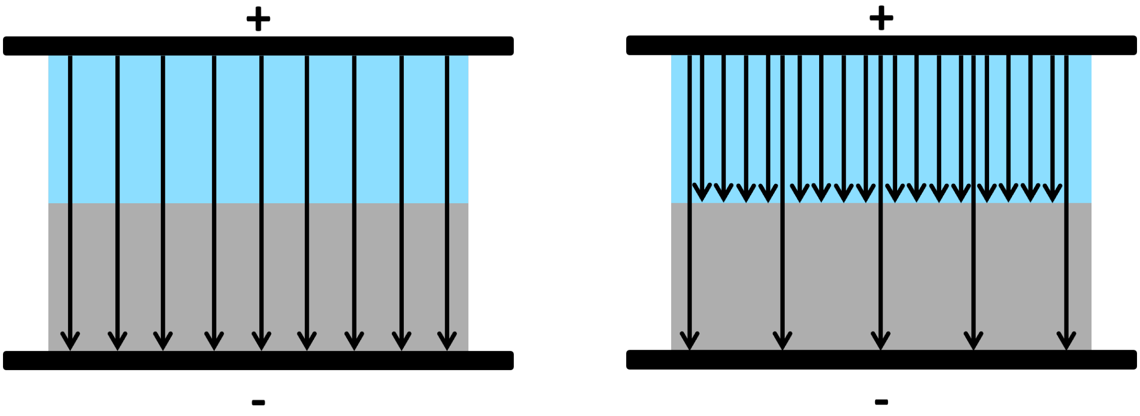

Figure 2.3: Field distribution in a two-layer stack with similar permittivities but different conductivities. (a) AC: the field splits evenly. (b) DC: the field concentrates in the lower-conductivity layer (layer 2).

This is the reason why the electrical material properties strongly influence the field distribution, which is especially relevant when testing solid plate samples surrounded by an insulating liquid: in the worst case, the electric field can be pushed into the liquid instead of into the material under test, giving misleading breakdown results.

2.2.3 Applied voltage characteristics

The waveform (AC, DC, lightning impulse), its rate of rise, and its polarity all affect the field indirectly, by determining how much time is available for conduction currents, space charge, and thermal effects to redistribute the initial capacitive field before breakdown occurs. A fast impulse effectively freezes the capacitive (ε-controlled) distribution; a slow DC ramp allows partial migration toward the conductive (σ-controlled) distribution; polarity affects the sign and mobility of accumulated space charge at electrode and interface boundaries.

2.2.4 Environmental and material-condition factors

Temperature affects both ε_r'' (loss) and σ directly, and therefore shifts the balance between the AC and DC field pictures described above. For solid insulation specifically, geometric defects (voids, delamination, an uncontrolled triple point) and embedded contaminants locally distort the field exactly as a sharp electrode would, effectively lowering η at that point regardless of the nominal test-cell geometry. For liquid insulation, dissolved water/moisture, entrained air bubbles or cavities, and metallic or fibrous contaminants each act as a local permittivity or conductivity discontinuity and are the dominant practical determinants of scatter in liquid breakdown data (2.4.2, 2.4.3).

2.3 Breakdown in Solid Insulation

The solid insulation material in this project, filled EPDM and unfilled EPDM, are used to stop the electric field from finding a path through the material. Breakdown is what happens when the material fails at that job and a conducting path forms anyway. There is more than one way this can happen, and which one dominates depends mainly on how strong the field is and how long it is applied [1].

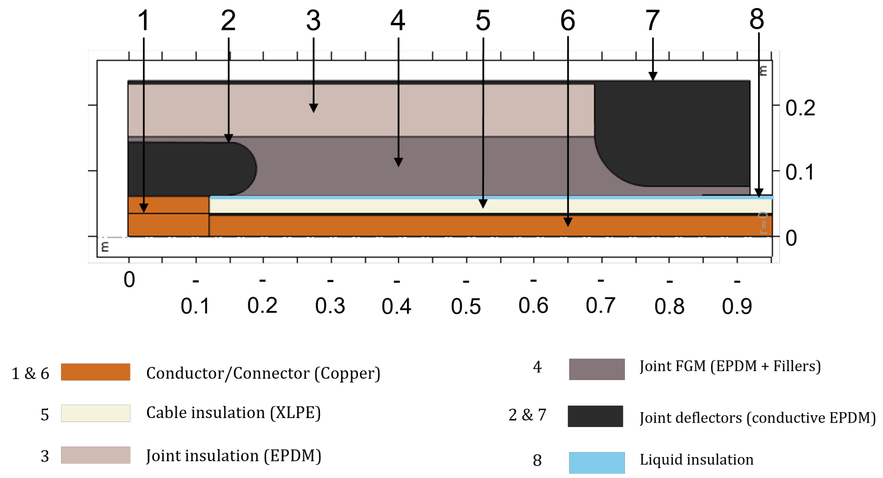

Figure 2.4: Cable Joint Cross-section [6]

Figure 2.4 shows a cross-section of a typical high-voltage cable joint, indicating the materials investigated in this thesis in the context of their actual location within an accessory. The copper conductor and connector (1, 6) are surrounded by the cable's factory-applied XLPE insulation (5), which is interrupted at the joint and built up on site using the joint insulation (3), an unfilled EPDM material equivalent to the unfilled EPDM tested in this project. The conductive EPDM deflectors (2, 7) correspond to the semiconductive screen material on either side of the joint, while the joint FGM (4), an EPDM compound loaded with functional filler, provides resistive field grading at the cable-joint interface discussed in 2.1.2 and is equivalent to the filled EPDM (FGM) tested in this project. Finally, the liquid insulation (8) occupies the interface between the joint body and the cable insulation, corresponding to the silicone oil and silicone grease characterised in this thesis.
In high-voltage cable accessories, this liquid layer serves two practical purposes beyond its role as an insulating medium: it lubricates the interface, reducing friction and making installation of the joint onto the cable easier, and it fills any small air gaps or voids that remain at the interface during operation, which would otherwise act as localised field-enhancing defects. This figure illustrates why the solid and liquid materials studied separately in this project are, in service, present together at the same interface, and why the field-grading behaviour of the FGM layer is positioned specifically at the location of highest field concentration in the accessory.

2.3.1 Electrical breakdown

Every solid contains a small number of free electrons, usually from impurities or tiny defects in the material. If the field is strong enough, these electrons are accelerated so much that when they collide with an atom, they knock out another electron. Each of those new electrons can do the same thing. The number of free electrons grows very quickly, and once there are enough of them lined up across the gap, a conducting channel exists and the material breaks down. This whole process takes a fraction of a second.

Breakdown initiation depends strongly on electrode geometry and the dielectric property of the sample. A sharp edge, an embedded particle or a triple point (the spot where electrode, rubber, and surrounding oil all meet) pulls the field toward itself and the breakdown often begins there rather than somewhere in the bulk material, since these are the locations where the local field is most strongly enhanced above the nominal applied value. In a homogeneous material with no such defects, avalanche breakdown tends to originate wherever the field happens to be highest in the bulk, which for a quasi-uniform electrode geometry is typically at or near the centre of the electrode.

2.3.2 Electrical treeing and long-term degradation

Electrical breakdown, as described above, is a near-instant event. But polymeric insulation can also fail slowly, over weeks or years, at stresses well below what would cause immediate breakdown. The most studied form of this slow failure is electrical treeing: a branch-like network of narrow discharge channels that grows through the material from a point of field concentration, resembling the structure of a tree [7]. Treeing usually starts at a void, a contaminant, or a sharp defect, and it grows in stages- first as a few sparse branches, later as a denser, bush-like structure with the rate of growth increasing at higher voltage and higher frequency of the applied stress.

Despite extensive research, the initiation process of electrical treeing remains actively debated in the literature. Early explanations proposed that mechanical fatigue from the oscillating electrostatic force between charges was responsible but this was later shown to produce forces far too small to crack a polymer under normal operating stresses. Other proposed mechanisms include localised Joule heating, high-field impact ionisation, and "hot" electrons energetic enough to break polymer bonds directly. However, none of these fully explain why trees can begin at fields much lower than the short-term breakdown strength of the material, and without requiring a pre-existing void at the initiation point. In practice, some combination of these effects is usually assumed with the local field enhancement at a defect or triple point remaining the one factor all explanations are agreed on.

Once a tree has started, each individual discharge inside the branch network barely damages the material. Its not one single event. Its discharge after discharge are repeated over thousands of voltage cycles or held at DC voltage that slowly extends the branches until one of them finally bridges the full insulation thickness and initiates breakdown. This is exactly why a short breakdown test carried out on the plate and half-mould samples in this project cannot capture treeing-driven failure as it only shows the intrinsic strength of the material and its sensitivity to defects on the timescale of seconds. Treeing and degradation only becomes visible over a properly designed endurance test running for a much longer period.

2.3.3 Thermal breakdown

Every material heats up a little when current flows through it. Normally this heat escapes into the surroundings and the sample settles at a stable temperature. The problem is that most polymers conduct better as they get warmer. So if heat cannot escape fast enough, the sample heats up, conducts more, and heats up further. If this loop is not interrupted, it ends in thermal breakdown sometimes at a field well below what would be needed for electrical breakdown alone.

$$q = \sigma E^2 + \omega \varepsilon_0 \varepsilon_r'' E^2 \tag{2.11}$$

Equation (2.11) gives the heat generated per unit volume of material, where σ is the conductivity, E the local field, ω the angular frequency, and ε_r'' the loss part of the permittivity. Filled EPDM (FGM) is affected by this more than unfilled EPDM, because FGM is designed to start conducting sharply once the field passes the switching threshold (2.3.4). It generates more heat under the same conditions, which matches the higher temperature rise simulated on the FGM samples compared with unfilled EPDM.

2.3.4 Nonlinear conduction and thermal behaviour of FGM

FGM is not a homogeneous material. It is EPDM rubber loaded with conductive or semiconductive filler particles (commonly ZnO or SiC) and its field-grading behaviour comes directly from how the particles are arranged inside the polymer and not from the base rubber itself [8, 9]. At low field, the filler particles are electrically isolated from one another by thin gaps or oxide layers, so very little current can pass and the composite behaves close to an insulator. As the field rises past a threshold often called the switching field charge carriers begin to tunnel or hop across these inter-particle gaps in large numbers, and the composite's conductivity increases sharply, sometimes by several orders of magnitude over a narrow field range. This threshold-and-jump behaviour is what allows a thin FGM layer to absorb a local field concentration that would otherwise sit unrelieved on the bulk EPDM insulation.

This same mechanism is the direct cause of the extra self-heating as in 2.3.3. Once the local field exceeds the switching threshold, the material is, by design, carrying meaningfully more current than an unfilled rubber would at the same field and that current dissipates as heat exactly where the field is highest. Filler type, particle size, and how evenly the filler is dispersed through the rubber all shift where the switching threshold sits and how sharp the transition is, which is one reason FGM samples from the same production batch can still show more spread in their breakdown results than plain EPDM.

2.3.5 Partial discharge and erosion

Real samples are rarely perfect. A small void can be trapped inside the rubber, or a thin gap can be left at an interface during moulding. The breakdown strength of air, approximately 25 kV/mm at 1 bar, is typically much lower compared to rubber materials, so the field inside such a gap ends up much higher than the field in the surrounding material. As a result, the gap discharges long before the rest of the sample is anywhere close to failing.

On its own, each of these tiny discharges barely damages the material. But they repeat, over and over, and slowly burn small cavity into the surface. Over time, these cavity connect into branching channels that work their way through the sample. This process is slow and gradual, nothing like the near-instant electrical breakdown described above.

2.3.6 Ageing

Even with no discharge activity at all, insulation slowly loses strength over its working life. Oxidation, moisture uptake, and general chemical degradation of the polymer all play a part. For unfilled EPDM, the field-grading behaviour of the filler material can also drift over time. This kind of long-term degradation is often summarised with a simple relationship between the material's lifetime and the applied stress,

$$t\,E^n \approx \text{constant}, \tag{2.12}$$

where the exponent n depends on the material and how well it was manufactured [1]. A short breakdown test cannot show this kind of failure it only reveals the intrinsic strength of the material and how sensitive it is to defects. Ageing only shows up in a proper endurance test, run over a much longer period.

2.4 Breakdown in Liquid Insulation

The liquid insulation materials in this project, silicone oil and silicone grease, serve two purposes: a lower-viscosity silicone oil is used to prevent flashover around the solid samples during testing, and both liquids act as the lubricant that sits at the cable accessory interface in a real accessory

2.4.1 Intrinsic breakdown

A very clean liquid can break down the same way as a solid. Free electrons gain energy from the applied electric field and upon colliding with molecules, can release additional electrons. This process can develop into an avalanche, setting an upper limit on the dielectric strength of the liquid. However, this is rarely the actual cause of failure in a real, technical-grade liquid. In practice, contamination is the dominant cause of breakdown.

2.4.2 Particles in the liquid

Dust or fibres suspended in the oil are pulled toward the region of highest field, since they are more easily polarised than the liquid around them. Once there, they can line up end to end and form a bridge across the electrode gap. This bridge concentrates the field further at its tip, and breakdown usually starts from that point. Clean, well-filtered oil avoids this entirely, which is why liquid cleanliness matters just as much as the liquid's own intrinsic strength.

2.4.3 Bubbles and cavities

A trapped gas bubble in the liquid experiences a stronger field than the liquid surrounding it. For a spherical bubble, the field inside it is approximately

$$E_{\text{bubble}} = \frac{3\,\varepsilon_{r,\text{liq}}}{1 + 2\,\varepsilon_{r,\text{liq}}}\,E_0, \tag{2.13}$$

where E_0 is the field that would exist in the liquid on its own, and $\varepsilon_{r,\text{liq}}$ is the liquid's relative permittivity. Since gas breaks down at a much lower field than liquid does, the bubble discharges first, and that discharge can be enough to trigger breakdown of the whole gap. This is why the test cell is filled carefully and degassed. A leftover bubble is a built-in weak point that has nothing to do with the actual strength of the oil being tested.

2.4.4 Streamers

Under a fast-rising voltage, breakdown in a liquid usually proceeds through a streamer which is a a narrow, fast-growing channel that starts at the high-field electrode and tries to cross the gap. A streamer does not grow at a single fixed speed. As the applied voltage is increased, its growth rate does not rise smoothly but jumps between a small number of distinct factors, which the literature labels, in order of increasing speed, as the 1st, 2nd, 3rd and 4th streamer modes [10]. In practice these are usually grouped into two behaviours: a slower regime (1st/2nd mode), where the streamer grows as a thin, sparsely branched filament at a few kilometres per second, and a much faster regime (3rd/4th mode), where growth can be one to two orders of magnitude quicker and the channel branches far more densely. The voltage at which a streamer switches from the slow regime to the fast one is called the acceleration voltage, and it marks the point where a small further increase in voltage produces a disproportionately large jump in how quickly the streamer can cross the gap.

At extremely short pulse durations, an additional mechanism has been proposed. The field gradient itself physically pulls the liquid apart (an electrostrictive effect). This creates elongated, nanoscale voids that then provide the starting point for an avalanche. This mechanism only becomes relevant at timescales far shorter than the DC and slow-ramp tests used in this project.

What matters most for interpreting the results in this thesis is that whether a streamer, once started, simply crosses the gap or instead stalls partway depends on the electric field uniformity introduced in 2.1.2. In a near-uniform field (small field factor), such as the sphere-to-plate geometry used for the plate samples, a streamer that starts usually carries straight across so the breakdown voltage is close to the voltage needed to start it in the first place. In a sharper, more divergent field, a streamer can start, stall partway across, and need extra voltage before it finally bridges the gap [5]. This difference is worth keeping in mind when comparing results from different electrode shapes in this project, even though the tests here are DC and slow-ramp rather than impulse.

3

Experimental Methodology

3.1 Weibull Analysis

The dielectric breakdown of polymeric insulation is inherently stochastic in nature, resulting in variations in breakdown strength although identical materials from same batch are tested under identical conditions. These variations arise from microscopic defects, impurities, voids or any other inhomogeneities that can cause local field enhancements that influence the initiation and propagation of breakdown mechanism. Hence the breakdown strength of the insulation materials is commonly analysed using statistical methods rather than deterministic approaches.

Among the available models, the Weibull distribution has become one of the most widely used tools to describe the failure behaviour of insulating materials and for assessing the reliability of electrical insulation systems [11, 13, 12]. Its popularity stems from its mathematical flexibility and its ability to accurately represent a broad range of failure characteristics observed in insulation breakdown experiments. The Weibull distribution has been extensively applied in reliability engineering, lifetime assessment studies, accelerated aging tests, and dielectric breakdown investigations of insulation systems [13, 12].

The Weibull distribution was originally introduced by Waloddi Weibull in 1951 as a statistical distribution function capable of describing a wide variety of physical phenomena, including mechanical strength, fatigue life, and electrical insulation breakdown [11]. Since then, it has become a standard method for analysing dielectric breakdown data because it provides a convenient framework for quantifying the probability of failure and evaluating the dispersion of experimental results.

In this analysis, the random variable may represent time to failure, breakdown voltage, electric field strength or any other quantity associated with a failure event. In our study, the random variable we deal with is breakdown field strength since our objective is to evaluate the dielectric strength of the investigated insulation samples for both solid and liquid insulation materials. The two-parameter Weibull distribution is characterized by the scale parameter, α, and shape parameter, β. The scale parameter defines the characteristic value of the distribution, whereas the shape parameter describes the statistical scatter of the measured breakdown strengths.

The cumulative probability of failure is described by the Weibull cumulative distribution function (CDF):

$$P_f(E) = 1 - \exp\left[-\left(\frac{E}{\alpha}\right)^{\beta}\right] \tag{3.1}$$

Where

- $P_f(E)$ is the cumulative probability of failure;
- E is the breakdown field strength;
- α is the Weibull scale parameter, commonly referred to as the characteristic breakdown field;
- β is the Weibull shape parameter.

The cumulative probability of failure represents the fraction of specimens that are expected to fail at or below a given breakdown field strength. As the applied electric field increases, the probability of failure approaches unity, indicating that an increasing proportion of specimens are expected to experience dielectric breakdown.

When the breakdown field strength is equal to the characterisitic value, i.e., $E = \alpha$, Equation (3.1) simplifies to

$$P_f(\alpha) = 1 - \exp(-1) = 0.632 \tag{3.2}$$

Which corresponds to cumulative failure to be around 63.2%

Thus, the characteristic breakdown field α is defined as the electric field strenth a which around 63.2% of the samples are expected to fail while the remaining 36.8% of the samples withstand this field and can survive beyond this field strength. This value provides a useful indicator for comparing the dielectric performance of different insulation systems and is commonly reported in the Weibull-based breakdown studies.

In addition to characteristic breakdown field, the shape parameter β provides information regarding the statistical dispersion of the experimental data. A high β value indicates a narrow distribution hence more consistent breakdown and behaviour among the sample. Conversely, a lower β value indicates greater scatter in breakdown results, suggesting a larger variability in insulation performance. As a result, both α and β are required to fully characterize the dielectric breakdown behaviour of an insulation system.

For the breakdown measurements presented in this thesis, the Weibull distribution was fitted to the experimentally obtained breakdown field strengths. The extracted values of α and β were subsequently used to compare the dielectric performance, reliability, and breakdown consistency of the investigated insulation materials in their test environment.

3.2 COMSOL Multiphysics Modelling

To complement the experimental breakdown tests and to verify the field behaviour predicted by the analytical expressions in Chapter 2, numerical simulations were performed using COMSOL Multiphysics. FEM modelling is widely used for analysing electric stress in insulation systems, particularly where field inhomogeneity and triple-point effects dominate [3, 4, 14]. The modelling approach follows the principles used in earlier EPDM/FGM studies [15], but is adapted to the geometries and materials developed in this thesis.

3.2.1 Simulation Objectives

Electric field simulations were carried out for each electrode configuration used in the breakdown tests, with three objectives:

- To evaluate the electric field distribution across the sample and surrounding medium.
- To identify the location of maximum field stress, confirming whether it occurs at the triple point (plate samples), at the electrode edge, or within the bulk material (moulded samples and liquid cell).
- To quantify the theoretical maximum field values used to compute the Schwaiger factor for the liquid test cell, enabling comparison between simulated and analytical field utilisation.

These simulations provide the theoretical basis for interpreting the breakdown behaviour presented in the results and discussion chapter.

3.2.2 Model Geometry and Physics

All simulations were performed using a two-dimensional axisymmetric geometry as seen in figures 3.1, 3.2 and 3.3. This exploits the rotational symmetry of the sphere–plate, mushroom–plate, and sphere–sphere electrode configurations, reducing the computational cost while preserving full accuracy. This choice is consistent with analytical field solutions introduced in Chapter 2 and with standard FEM practice [16]. Two physics interfaces were coupled:

- **Electric Currents (EC)** to compute the electric field distribution under AC and DC excitation.
- **Heat Transfer (HT)** to capture temperature rise due to dielectric losses and conduction currents, particularly relevant for FGM due to its nonlinear conductivity [17, 3].

A time-dependent voltage ramp was applied to the high-voltage electrode, matching the experimental procedure. Ramp rates were set to 0.5 kV/s for FGM and 2 kV/s for EPDM, consistent with the breakdown methodology described in Section 3.1.

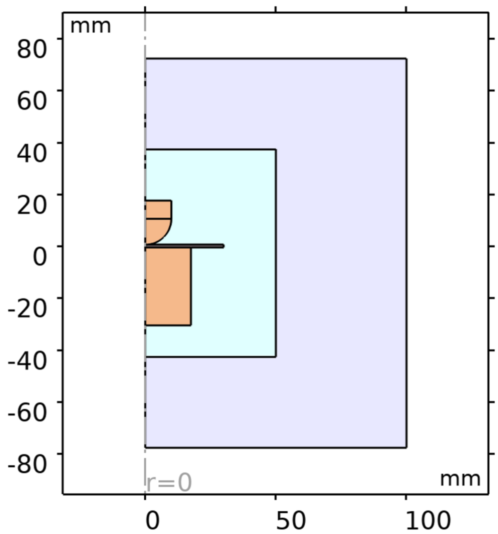

(a) FGM Plate

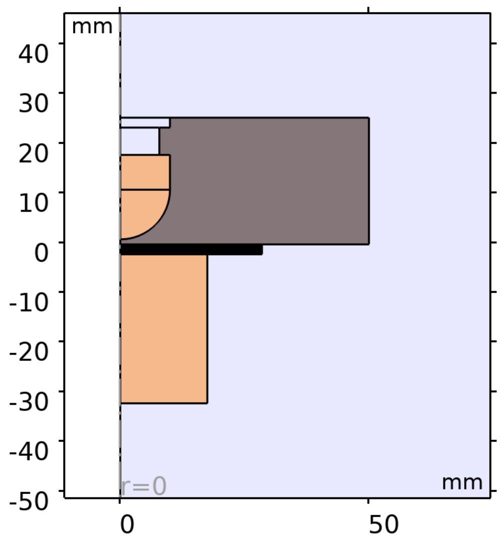

(b) FGM Half-Mould

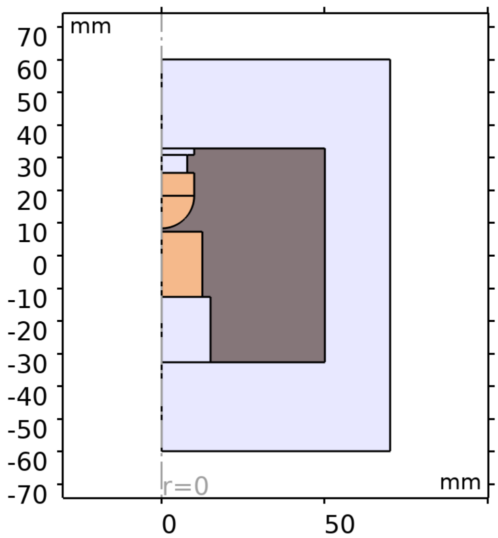

(c) FGM Full-Mould

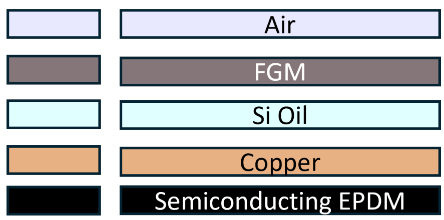

(d) Material legend

Figure 3.1: Solid insulation sample configurations used in the FGM simulations (sphere-plate electrodes): (a) plate, (b) half-mould, and (c) full-mould geometries. The material legend is shown in (d).

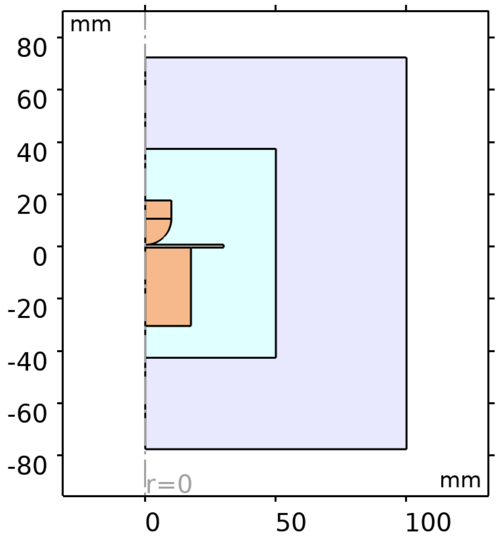

(a) EPDM Plate

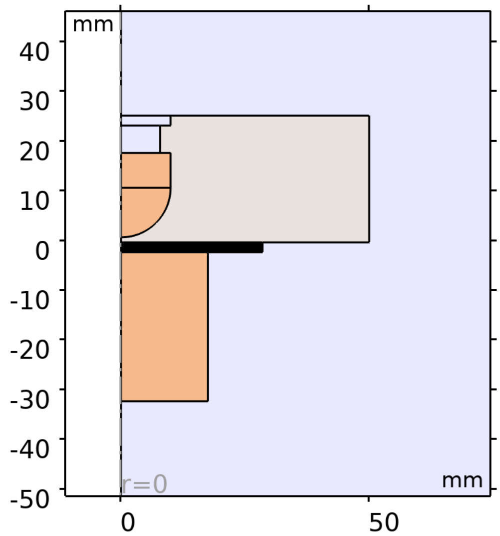

(b) EPDM Half-Mould

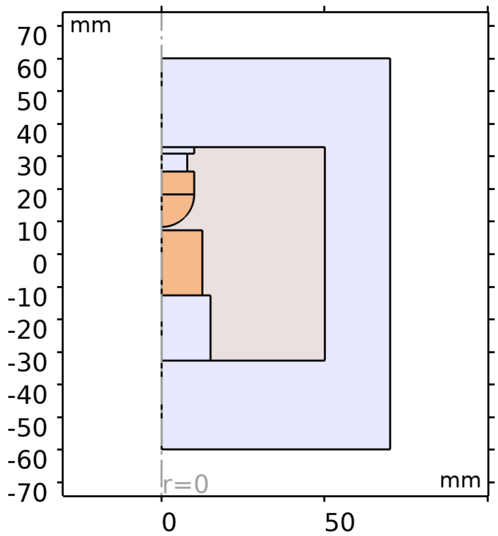

(c) EPDM Full-Mould

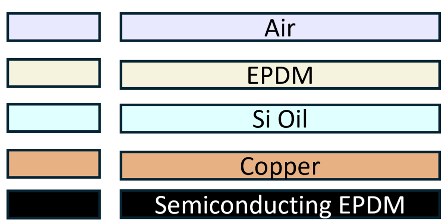

(d) Material legend

Figure 3.2: Solid insulation sample configurations used in the EPDM simulations(sphere-plate electrodes): (a) plate, (b) half-mould, and (c) full-mould geometries. The material legend is shown in (d).

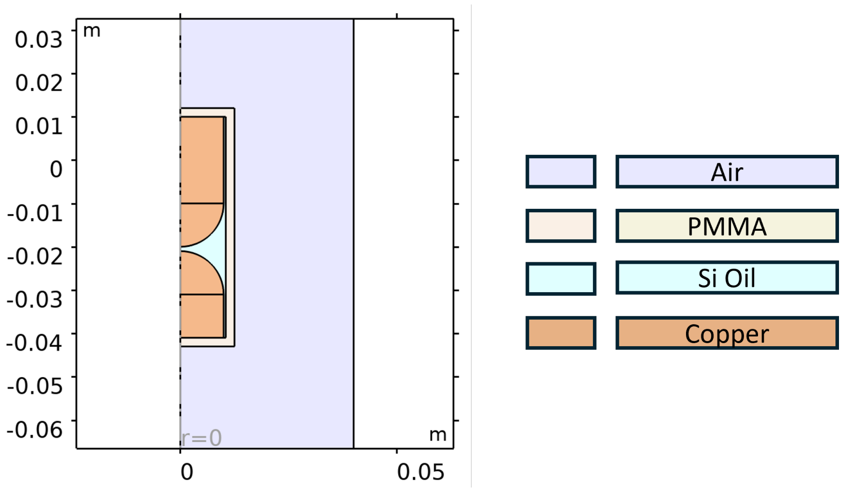

Figure 3.3: Liquid insulation sample configurations used in the simulations(sphere-plate electrodes) with material legend.

Table 3.1 summarizes the combinations of material, sample/electrode configuration, and voltage type covered by the breakdown tests described in this chapter.

Table 3.1: Summary of breakdown tests carried out in this project.

Material	Configuration	Voltage type	Ramp rate
Filled EPDM (FGM)	Plate	DC	0.5 kV/s
Filled EPDM (FGM)	Half-mould	DC	0.5 kV/s
Filled EPDM (FGM)	Full-mould	DC	0.5 kV/s
Unfilled EPDM	Plate	DC	2 kV/s
Unfilled EPDM	Half-mould	DC	2 kV/s
Unfilled EPDM	Full-mould	DC	2 kV/s
Silicone oil	Sphere-to-sphere cell	AC / DC	0.5 kV/s
Silicone grease	Sphere-to-sphere cell	AC / DC	0.5 kV/s

3.2.3 Boundary Conditions and Material Models

The high-voltage electrode was assigned a time-dependent potential $V(t)$, while the opposite electrode was grounded. External boundaries were placed sufficiently far from the electrodes to ensure negligible field influence and were set as electrically insulating. Continuity of normal current density was enforced at all material interfaces.

Thermal boundaries were held at ambient temperature, with internal heat generation given by

$$q = \sigma(E,T)E^2 + \omega\varepsilon_r''E^2,$$

as introduced in Section 2.3.3

Material models were defined as follows:

- **EPDM**: low conductivity, weak temperature dependence, negligible dielectric losses [18].
- **FGM**: nonlinear conductivity $\sigma(E, T)$ exhibiting a sharp increase once the switching field is exceeded, leading to localised heating and potential thermal runaway [17, 18].
- **Silicone oil and grease**: homogeneous permittivity, with breakdown behaviour governed by liquid mechanisms described in [3].

3.2.4 Meshing Strategy

A refined mesh was applied at the electrode edges, the triple point, and the custom gap, where strong field gradients are expected. Triple-point stress concentration is well documented in dielectric systems [4, 14]. Mesh independence was verified by ensuring that the maximum field E_{max} changed by less than 2% upon refinement [16].

3.2.5 Electrode Configurations

The following geometries were simulated to match the experimental setups:

- **Plate samples**: sphere-plate (DC) and mushroom–plate (AC), chosen to maintain a quasi-uniform field.
- **Moulded samples**: sphere-plate embedded in EPDM or FGM, used to study the influence of electrode embedding and triple-point stress.
- **Liquid samples**: spheresphere electrodes immersed in silicone oil or grease, producing a nearly homogeneous field like in other type of configurations discussed.

3.2.6 Electric Field Distribution

The simulations confirm that the highest electric field occurs at the triple point for plate samples, consistent with the analytical discussion in 2.3.1. For unfilled EPDM, the field distribution remains close to capacitive (permittivity-controlled) due to its low electrical conductivity and since the relative permittivity of unfilled EPDM is similar to that of the surrounding oil and grease, the field is not strongly redistributed at the material interface, and the temperature rise is minimal. For FGM, the field distribution instead becomes resistive (conductivity-controlled) at higher fields, once the nonlinear conductivity increases sharply above the switching threshold; because the electrical conductivity of FGM differs from that of the surrounding liquid by orders of magnitude at these fields, this produces strong field enhancement in the bulk material, and the resulting nonlinear conduction leads to significant local heating and eventual thermal runaway concentrated in the bulk, between the two electrodes, rather than at the triple point.

In the liquid test cell, the sphere-sphere geometry produced a nearly uniform field. The field utilisation was quantified using the Schwaiger factor $\eta = E_0/E_{\max}$, where $E_0 = V/d$ is the mean (nominal) field obtained from the applied voltage V and the nominal electrode gap $d = 1$ mm, and $E_{\max}$ is the maximum field obtained from the COMSOL simulation at that same voltage. The resulting simulated field values and the corresponding Schwaiger factor for the finalized liquid test cell are reported in 5.2.1.

3.2.7 Thermal Behaviour of FGM

Time-dependent simulations show that FGM experiences rapid temperature rise under DC stress due to its nonlinear conductivity. The heat generation term $\sigma(E,T)E^2$ increases sharply as the voltage ramps up, leading to localised heating in the bulk material, between the two electrodes, and eventual thermal instability, consistent with polymer breakdown theory [17, 18].

3.3 Relevant Standards for Breakdown Testing of Solid and Liquid Insulation Materials

Breakdown testing of insulation materials is governed by established international standards that define the electrode geometry, voltage application method, sample preparation, and criteria for breakdown. These standards ensure that measurements are comparable, repeatable, and representative of the dielectric behaviour of the material under controlled conditions. In this thesis, the procedures for both liquid insulation (silicone oil and silicone grease) and solid insulation (EPDM and FGM) are aligned with the principles of **IEC 60156**, **IEC 60243-1**, and **IEC 60243-2**, with modifications introduced to accommodate the specific research objectives and custom test-cell designs.

3.3.1 IEC 60156: AC Breakdown Testing of Insulating Liquids

IEC 60156 specifies the method for determining the AC breakdown voltage of insulating liquids at power frequency. It is widely used for acceptance testing of fresh insulating liquids, quality control of processed liquids, and condition assessment of liquids in service.

Key requirements include:

- **Electrode Geometry:** Spherical or partially spherical electrodes (12.5–13 mm diameter or 25 mm radius) to ensure a quasi-uniform electric field.
- **Electrode Gap:** A fixed spacing of 2.5 mm $\pm$ 0.05 mm.
- **Voltage Application:** A uniform rate-of-rise AC voltage until breakdown occurs.

- **Sample Handling:** The liquid must be free from bubbles, moisture, and suspended particles; stirring is recommended.
- **Breakdown Criterion:** Breakdown is defined as a sudden voltage collapse with a corresponding current surge.

Relevance to this work: The liquid test cell developed in this thesis follows the electrode geometry principles of **IEC 60156** but employs a *custom reduced gap*. This modification was introduced for two essential reasons:

- A smaller gap increases the nominal electric field for a given applied voltage, ensuring that breakdown occurs well within the maximum output capability of the laboratory test equipment. This prevents the voltage supply from reaching its upper limit.
- A reduced gap minimizes the risk of surface flashover along the cell walls or electrode supports. Flashover becomes more likely when the applied voltage approaches the equipment limit or when the geometry introduces unintended field enhancement.

These adjustments allow the test cell to remain consistent with the principles of **IEC 60156** while providing a geometry suitable for high-viscosity liquids and small-volume research samples.

3.3.2 IEC 60243-1: Electric Strength of Solid Insulating Materials (AC Tests)

IEC 60243-1 defines test methods for determining the short-time AC breakdown strength of solid insulation materials. It covers boards, sheets, films, moulded materials, and shaped insulating components.

Key requirements include:

- **Electrode Configurations:** Sphere–plate, cylinder–plate, or parallel-plate electrodes depending on material type.
- **Surrounding Medium:** Tests may be conducted in air, oil, or other liquids.
- **Voltage Application:** Rapid-rise AC tests, step-by-step tests, and slow rate-of-rise tests (120–240 s).
- **Breakdown Criterion:** Breakdown is detected by a sudden current increase or flashover.

Relevance to this work: The solid insulation tests (EPDM and FGM) in this thesis follow the sphere–plate configuration recommended by **IEC 60243-1**. For thermosets and elastomers specifically, the standard itself recommends a sample thickness of around 1 mm, rather than the 3 mm or more typical for boards and sheets; the gap distance used in this project (approximately 1 mm, 4.2.4) is therefore consistent with the standard's own recommendation for this material class, and was selected because cable accessory interfaces operate with thin insulation layers, field-grading materials are designed for high-stress small-gap regions, and triple-point behaviour becomes more pronounced at smaller distances.

A gap consistent with this recommendation was therefore selected to:

- replicate realistic interface geometries found in cable joints and terminations,
- ensure breakdown occurs below the voltage limit of the test equipment,
- avoid surface flashover in moulded samples,
- increase sensitivity to triple-point stress and local field distortion, since for a fixed applied voltage a smaller gap raises the nominal field strength, which makes any local field enhancement at a defect or triple point proportionally more significant relative to the surrounding uniform field.

3.3.3 IEC 60243-2: Electric Strength Under DC Stress

IEC 60243-2 provides additional requirements for DC breakdown testing of solid insulation. It is particularly relevant for materials where conductivity is field-dependent, space-charge accumulation influences breakdown, or thermal runaway is possible under DC stress.

Key requirements include:

- **Voltage Source:** Smooth, ripple-free DC voltage with controlled rate of rise.
- **Voltage Distribution:** Under DC, the field distribution evolves from capacitive to resistive as conduction currents and space charge develop.
- **Breakdown Behaviour:** DC breakdown voltages are typically higher than AC breakdown voltages, especially for non-homogeneous materials.

Relevance to this work: FGM exhibits nonlinear conduction and field-dependent conductivity, making DC testing essential. The DC ramp tests (0.5 kV/s for FGM and 2 kV/s for EPDM) align with the slow rate-of-rise methodology described in **IEC 60243-2**.

The custom reduced gap again plays a critical role by:

- increasing the sensitivity of the test to thermal runaway,
- ensuring breakdown occurs within the voltage capability of the DC supply,
- reducing the likelihood of flashover in oil-immersed plate samples,
- enabling moulded samples to mimic real accessory geometries.

3.3.4 Summary

IEC and ASTM standards do not mandate a single fixed electrode gap for breakdown testing, and the recommended range differs by material class.

For **liquid insulation**, **IEC 60156** [19] specifies a fixed gap of 2.5 mm, while the corresponding ASTM standard, **ASTM D1816**, specifies electrode gaps of 2 mm and 1 mm [20]. The 1 mm gap used in the liquid test cell in this project falls within this range.

For **solid insulation**, **IEC 60243-1** [21] recommends approximately 1 mm for thermosets and elastomers specifically, rather than the 3 mm or more typical for boards and sheets, while **ASTM D149** similarly does not mandate a single fixed gap and commonly permits specimen thicknesses in the 0.8-3.2 mm range [22]. The approximately 1 mm gap used for the solid samples in this project falls comfortably within this range.

The gap distances used in this thesis (1 mm for the liquid test cell and approximately 1 mm for the solid samples) therefore fall within, or close to, the range recommended by IEC and ASTM for the respective material classes tested, rather than representing an arbitrary deviation introduced specifically for this research. This choice was motivated by the need to replicate high-stress regions found in cable accessories, prevent surface flashover, remain within the voltage limits of the test equipment, minimize sample volume, and ensure compatibility with the moulded sample geometries and COMSOL simulation models. These gap distances enable controlled, repeatable, and representative breakdown testing for both solid and liquid insulation materials.

4

Experimental Setup

This chapter describes the materials, test-cell designs, electrode configurations, and sample preparation procedures used for the breakdown testing carried out in this project. It also documents the iterative process by which the finalized solid-sample mould and liquid test cell were reached, since the intermediate designs and their specific shortcomings are what motivate several of the design choices described here used to evaluate the electric field distribution for each configuration.

4.1 Materials

Two solid and two liquid insulation materials are tested in this project, reflecting the two material categories present at the interface inside a real cable accessory: the bulk and field-grading rubber insulation, and the lubricant/insulating liquid that sits between the rubber and the cable during installation and service.

4.1.1 Solid insulation materials

4.1.1.0.1 Unfilled EPDM: Ethylene propylene diene monomer (EPDM) rubber, without additional functional (field-grading) fillers, is used as the bulk insulation material. Note that "unfilled" here refers specifically to the absence of these functional fillers; like any standard EPDM compound, the material still contains the usual processing ingredients and reinforcing fillers used in rubber compounding, and is not literally filler-free. EPDM is widely used in high-voltage cable accessories because of its combination of dielectric strength, thermal stability, and mechanical flexibility, which allows pre-moulded accessory components to maintain a stable interface with the cable under mechanical and thermal cycling in service.

4.1.1.0.2 Filled EPDM (FGM): The field-grading material used in this project is an EPDM rubber compound loaded with conductive or semiconductive functional fillers. Unlike unfilled EPDM, filled EPDM (FGM)'s electrical conductivity is strongly and non-linearly dependent on the local electric field: below a threshold field it behaves close to an insulator, and above that threshold its conductivity increases sharply, allowing it to relieve local field concentrations that would otherwise appear at geometric discontinuities such as the cable screen cut-back point 2.1.

This behaviour, and its consequences for thermal and breakdown performance, is discussed in 2.3.4.

Table 4.1: Solid insulation materials tested.

Material	Type	Role in this project
Unfilled EPDM	Bulk insulation	Reference/baseline solid material
Filled EPDM (FGM)	Field-grading material	Stress-control material

4.1.2 Liquid insulation materials

4.1.2.0.1 Silicone oil: Two distinct silicone oils are used in this project, and it is important to distinguish between them. A low-viscosity silicone oil is used only as the surrounding medium during solid-sample breakdown testing 4.2, to suppress surface flashover around the sample; this oil is not itself characterised as a dielectric material in this thesis. A separate, considerably higher-viscosity silicone oil comparable in application to the lubricant used at a real cable-accessory interface is tested in its own right as an insulating liquid using the finalized liquid test cell 4.3.1.

4.1.2.0.2 Silicone grease: Silicone grease is used at the rubber-to-cable accessory interface in real accessories as an installation lubricant, alongside the higher-viscosity silicone oil described above, and is tested in this project as an insulating material in its own right using the same finalized liquid test cell 4.3.1. Its substantially higher viscosity compared with the low-viscosity surrounding-medium oil was one of the driving requirements behind the finalized test-cell design, discussed below.

Table 4.2: Liquid insulation materials tested.

Material	Consistency	Role in this project
Silicone oil	Low-viscosity liquid	Surrounding medium
Silicone oil	High-viscosity liquid	Interface lubricant / standalone dielectric
Silicone grease	High-viscosity semi-solid	Interface lubricant / standalone dielectric

4.1.3 Physical form and handling

The four materials tested in this project require different handling procedures given their different physical forms. Unfilled EPDM and filled EPDM (FGM) are supplied as an uncured or partially cured rubber compound that is shaped into its final sample form only during the moulding process described in 4.2.4; consequently, sample consistency depends as much on correct moulding procedure as it does on the base material itself. Silicone oil, being a free-flowing liquid, is injected directly into the test cell, while silicone grease, being a high-viscosity semi-solid, does not flow or self-level in the same way and required specific handling consideration when the finalized liquid test cell was designed 4.3.1, since trapped air bubbles are considerably harder to remove from a high-viscosity material such as grease than from a free-flowing liquid such as oil.

4.2 Solid Insulation Test Setup

4.2.1 Sample types

Three sample and electrode configurations are used for the solid insulation tests, chosen to separate the intrinsic breakdown strength of the material from the influence of electrode geometry and the triple point discussed in 2.3.1.

4.2.1.0.1 Plate sample: A flat, moulded plaque of EPDM or filled EPDM (FGM) is tested with the high-voltage and ground electrodes resting against its flat surfaces, with the whole assembly immersed in the surrounding insulating liquid. This is the configuration in which the triple point - electrode, solid, and liquid all meeting at one location is most pronounced, since the electrode is not embedded in the material at all.

4.2.1.0.2 Half-mould sample: The high-voltage electrode is embedded directly into the rubber during moulding, while the ground side remains external. This partially reduces the triple point compared with the plate configuration, since only one electrode interface is now embedded, while the sample is still tested immersed in liquid.

4.2.1.0.3 Full-mould sample: Both electrodes are embedded directly into the rubber during moulding, eliminating the electrode-solid-liquid triple point entirely. The full-mould configuration is therefore the closest representation of the material's intrinsic breakdown strength, uninfluenced by an external liquid interface, though at the cost of a substantially more demanding moulding process as described in section (4.2.4).

4.2.2 Electrode configuration

Plate samples immersed in oil are tested with a sphere-to-plate electrode arrangement under DC and a mushroom-to-plate (rounded high-voltage electrode over a flat ground plate) arrangement under AC. Both geometries are chosen to keep the field close to uniform (2.1.2) at the sample surface, avoiding an artificial field concentration that the material would not otherwise experience, while still defining a single, repeatable maximum-stress location for consistent breakdown initiation.

Moulded (half- and full-mould) samples are tested with a sphere-to-plate electrode arrangement under DC, with the sphere electrode embedded directly in the rubber.

4.2.3 Rationale for electrode geometry selection

The choice of electrode geometry as seen in figures 3.1, 3.2, and 3.3 for each sample type follows directly from the field-uniformity framework introduced in 2.1.2. For the plate configuration, a sphere or mushroom electrode is chosen specifically to keep the Schwaiger factor η close to unity, so that the measured breakdown voltage reflects the intrinsic strength of the EPDM or filled EPDM (FGM) sample itself rather than an artificial field concentration introduced by a sharp electrode edge. This matters most for the comparison between materials: since filled EPDM (FGM)'s field-grading behaviour is itself a response to local field concentration (2.3.4), testing it with an already-divergent electrode would confound the material's intrinsic grading response with an externally imposed field concentration, making the two effects impossible to separate.

For the moulded configurations, embedding the electrode directly in the rubber removes the triple point identified as the dominant failure location for plate samples (2.3.1), which is the entire purpose of the half- and full-mould designs: they isolate the question of *how much* the triple point affects the measured breakdown strength, by providing a same-material comparison where that specific defect source has been progressively removed. The difference in breakdown strength between the plate and moulded configurations for a given material is therefore attributable specifically to the triple-point effect, rather than to any other difference between the test conditions, since the electrode-to-sample geometry near the maximum-stress point is otherwise kept as similar as practically possible between configurations.

4.2.4 Sample preparation

Solid samples are prepared by moulding the rubber compound under heat and pressure using a hydraulic press. The finalized preparation procedure, following the mould design described in 4.4.1, consists of the following steps (see figure 4.1) below:

1. Weighing out the required quantity of rubber compound. The finalized mould design reduces the material quantity required compared with earlier iterations, owing to the grooves added to control material flow during pressing.

2. Positioning the electrode (for half- and full-mould samples) within the mould cavity, ensuring correct alignment before the mould is closed.

3. Filling the mould cavity with the weighed rubber compound, taking care to distribute the material evenly around the electrode to reduce the risk of trapped air.

4. Closing the mould and loading it into the hydraulic press.

5. Pressing the mould under controlled temperature and pressure for a fixed dwell time.

6. Allowing the moulded sample to cool before removal from the mould.

7. Removing the finished sample from the mould and visually inspecting it for defects in particular air cavities, delamination at the electrode interface, and confirming the target electrode-to-surface gap of approximately 1 mm is achieved.

8. Storing the prepared sample under controlled conditions until testing.

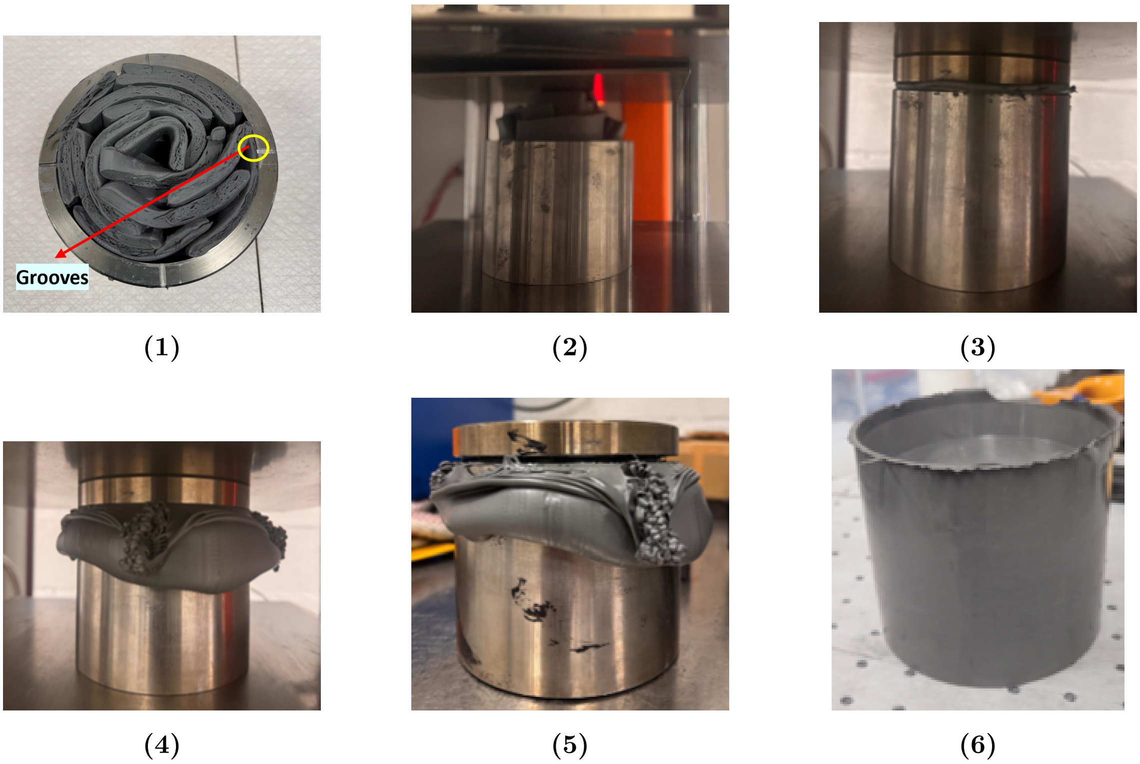

Figure 4.1: Solid sample preparation sequence.

4.2.5 Test procedure

Breakdown testing on solid samples follows a voltage-ramp procedure. For filled EPDM (FGM) samples, the DC voltage is increased at a rate of 0.5 kV/s; for unfilled EPDM samples, the DC voltage is increased at a rate of 2 kV/s. These ramp rates were chosen specifically so that, given the different characteristic breakdown voltages of the two materials, the total time to breakdown is approximately the same for both, keeping the test within the same "rapid-rise" rate-of-rise category defined by **IEC 60243-1** and **IEC 60243-2**, rather than one material being effectively tested under a slower, more time-dependent stress regime than the other. The ramp is continued until breakdown occurs, identified by a sudden collapse in the applied voltage and a corresponding current surge, at which point the voltage source is disconnected and the breakdown voltage is recorded.

4.2.6 Data acquisition and control

Applying a controlled voltage ramp and reliably detecting the moment of breakdown requires a measurement and control system with three functions: setting and executing the voltage ramp at the specified rate, continuously monitoring the applied voltage and current so that breakdown can be detected as soon as it occurs, and safely disconnecting the source once breakdown is detected.

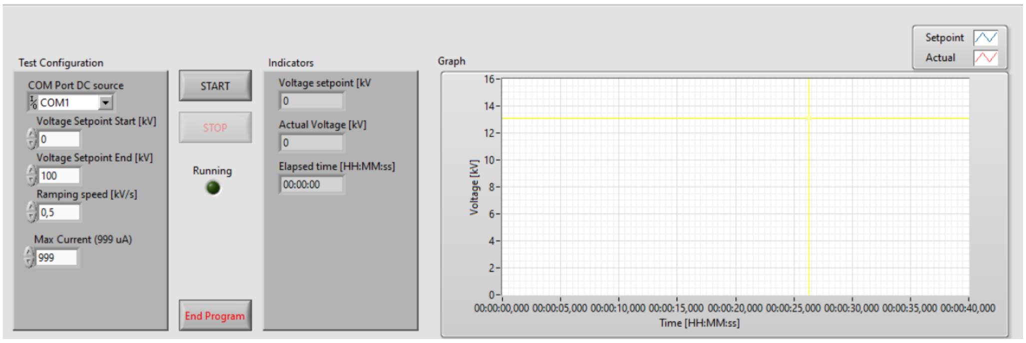

Figure 4.2: Control Unit-LABVIEW [15]

In a typical DC breakdown test setup of this kind, a programmable DC source is controlled via a software interface (commonly LabVIEW or an equivalent data-acquisition platform, see figure 4.2) that allows the operator to set the start voltage, end voltage, and ramp rate, and that logs voltage, current, and elapsed time throughout the test. Breakdown is identified automatically by the control software when the measured current exceeds a preset threshold or the voltage collapses suddenly, at which point the source is disconnected and the peak voltage immediately prior to the collapse is recorded as the breakdown voltage.

The test cell itself is enclosed within a protective cage during testing, both to prevent operator access to live high-voltage equipment and, in the case of the liquid test cell, to allow the transparent PMMA housing to be observed safely from outside the cage during the ramp.

4.3 Liquid Insulation Test Setup

4.3.1 Test cell design

The finalized liquid test cell as seen in figure 4.3 is constructed from PMMA (acrylic). PMMA was chosen for its electrical insulating properties and, equally importantly, its optical transparency, which allows the breakdown event and electrode condition to be observed directly during testing. The design was driven by five requirements, identified through the improvement trials described in 4.4.2:

- **Controlled gap distance** - the electrode spacing must be fixed and repeatable between tests, since gap distance directly affects the measured breakdown voltage.
- **Reduced fresh sample volume per trial** - particularly important given the cost and limited availability of some test liquids, and to allow a larger number of repeat tests within a fixed quantity of material.
- **Good visibility** - to allow direct observation of the breakdown location and any pre-breakdown activity (e.g. bubble formation, particle migration) described in 2.4.3 and 2.4.2.
- **Reliable breakdown of high-viscosity lubricants** - the cell must work as

reliably for silicone grease, which does not flow or settle the way silicone oil does, as it does for silicone oil itself.

- **Operating range** - the cell must withstand up to 100 kV under both AC (r.m.s.) and DC without external flashover along the PMMA housing itself.

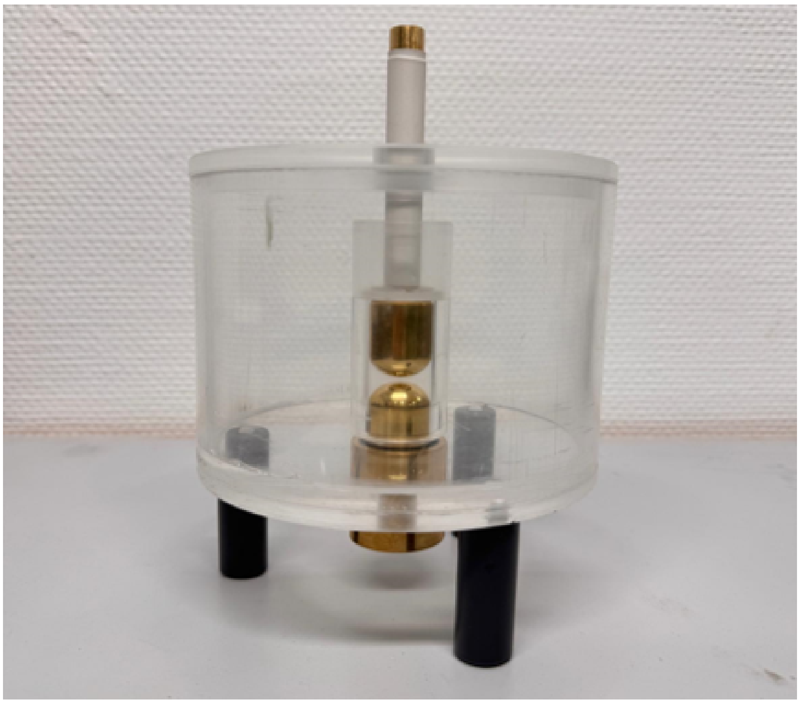

Figure 4.3: Final test cell design for liquid insulation

4.3.2 Electrode configuration

A sphere-to-sphere electrode arrangement is used for the liquid insulation tests under both AC and DC. This geometry is close to a homogeneous field. For the nominal electrode gap of $d = 1$ mm used in the finalized cell, taking an applied voltage of $V = 20$ kV as a representative example gives a mean (nominal) field of

$$E_0 = \frac{V}{d} = \frac{20 \text{ kV}}{1 \text{ mm}} = 20 \text{ kV/mm}. \tag{4.1}$$

Simulating the actual field distribution in the finalized cell at this applied voltage gives a maximum field of $E_{\max} = 20.7$ kV/mm, so the Schwaiger factor is

$$\eta = \frac{E_0}{E_{\max}} = \frac{20}{20.7} \approx 0.966, \tag{4.2}$$

confirming, per the classification in 2.1.2, that the cell produces a nearly homogeneous field ($\eta \approx 1$), so the measured breakdown voltage reflects the liquid's own intrinsic strength rather than an artefact of a sharp or divergent electrode geometry.

4.3.3 Rationale for electrode geometry selection

A sphere-to-sphere arrangement is used for the liquid tests rather than, for example, a needle-to-sphere or needle-to-plane geometry, because the objective of this part of the project is to characterise the liquids' breakdown strength under a uniform field 2.4.1, rather than their behaviour under an intentionally divergent field. Regardless of electrode shape, any measured breakdown voltage reflects a genuine breakdown property of the liquid itself; the choice of electrode geometry instead determines which type of breakdown strength is being measured the liquid's strength under near-uniform stress, as tested here, or its strength (and streamer behaviour) under a locally concentrated, non-uniform field, as would be tested with a divergent electrode. As discussed in 2.4.4, whether a streamer initiates and immediately bridges the gap, or instead initiates, stalls, and requires additional voltage to complete the breakdown, depends strongly on field uniformity; a near-homogeneous cell keeps the measured breakdown voltage close to the streamer initiation voltage under uniform-field conditions, which is the specific quantity of interest for comparing the liquids' bulk dielectric strength in this thesis. This is also why the field verification in Eq. (4.2) matters because confirming $\eta \approx 0.966$ for the finalized cell is what justifies treating the measured breakdown voltages as representative of liquid insulations under near-uniform field conditions specifically.

4.3.4 Sample preparation

Liquid samples are prepared and loaded into the test cell following a fixed procedure (as seen in figure 4.4) to minimise the risk of contamination or trapped air, both of which are known to reduce measured breakdown strength (2.4.2, 2.4.3):

1. Cleaning the test cell and electrodes before each fresh filling, to remove residue and breakdown traces from the previous test.
2. Positioning the sphere electrodes at the required gap distance.
3. Filling the cell with the liquid under test (silicone oil or silicone grease).
4. Visually inspecting the filled cell for trapped air bubbles before proceeding, given the good visibility requirement described in 4.3.1.
5. Allowing the sample to reach a stable condition before applying voltage.

4.3.5 Test procedure

Breakdown testing on liquid samples follows a voltage-ramp procedure at 0.5 kV/s, consistent with the ramp rate used for the FGM solid samples. The ramp is applied until breakdown occurs, identified by a sudden collapse in applied voltage, at which point the breakdown voltage is recorded. This represents one deliberate deviation from the standard **IEC 60156** procedure: for low-viscosity liquids, the standard typically permits repeated breakdowns on the same sample, either because the breakdown channel disperses naturally or because the liquid is stirred to bring fresh liquid between the electrodes before the next test. For the high-viscosity oil and grease tested in this project, this is not practical, since the breakdown channel and any resulting contamination do not disperse or redistribute on a comparable timescale; a fresh sample is therefore used for every individual breakdown test.

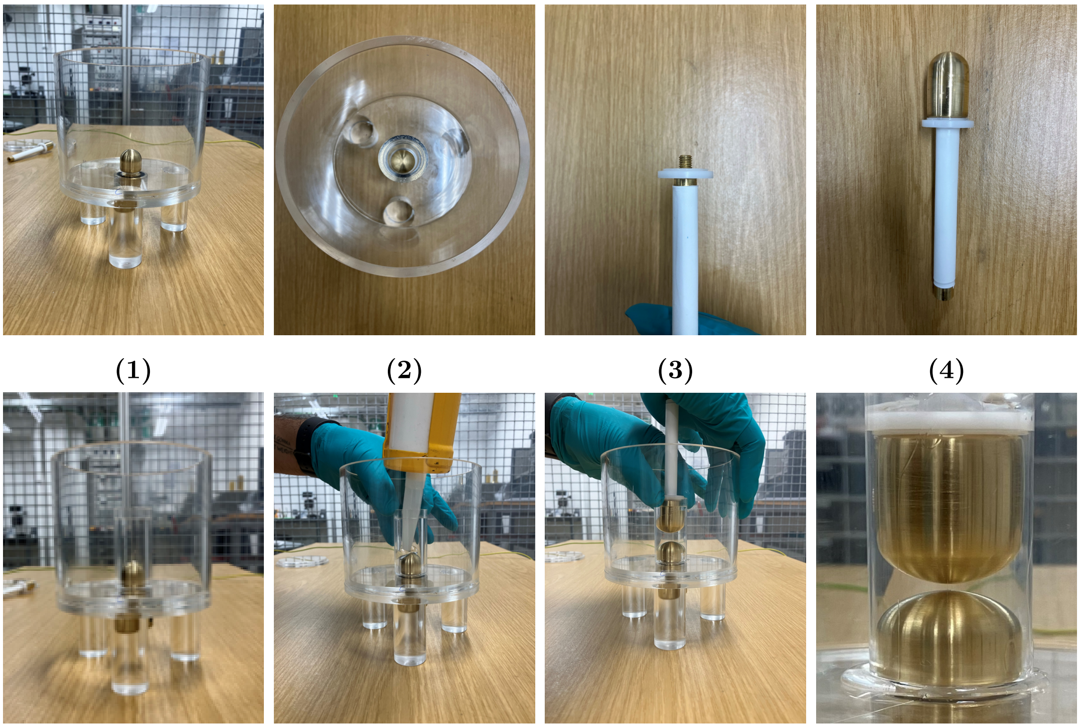

(1) (2) (3) (4)

(5) (6) (7) (8)

Figure 4.4: Liquid sample preparation sequence.

4.4 Test Setup Improvement Trials

Both the solid-sample mould design and the liquid test cell went through several iterations before reaching their finalized form. This section documents that process in detail, since the defects identified along the way rather than being discarded as failed attempts directly motivate the sample-preparation and test-cell requirements described in 4.2 and 4.3.

4.4.1 Solid insulation

4.4.1.0.1 First moulded sample. The first attempt at a moulded sample (as seen in figure 4.5a) showed two distinct problems. Air cavities were trapped within the rubber during moulding, which as in 2.3.5 create local regions of enhanced field that can discharge and erode the surrounding material well before the bulk rubber is anywhere near its own breakdown strength, making any breakdown result from this sample unrepresentative of the material's intrinsic strength. In addition, the moulding pressure and temperature had not yet been optimised for the geometry being used, contributing to inconsistent sample quality.

4.4.1.0.2 Refined mould preparation. A second iteration addressed the pressure and temperature settings, but introduced a new problem: delamination was observed at the rubber–electrode interface as seen in figure 4.5b, meaning the rubber did not adhere consistently to the embedded electrode surface across the full contact area. This is a serious defect for a moulded sample specifically, since a delaminated region behaves electrically like the void described in 2.3.5 a thin gap of much lower breakdown strength than the surrounding solid, sitting directly at the point of highest field. In addition, the electrode-to-surface gap was not yet consistently controlled at the intended 1 mm target, introducing sample-to-sample variability in the effective test geometry itself. These two problems motivated further work on both the material quantity used and the mould's internal design.

4.4.1.0.3 Finalized mould design. The finalized mould design resolved both issues by adding grooves to the mould cavity to control material flow during pressing allowing trapped air to escape more effectively during moulding rather than becoming sealed inside the sample while also reducing the total material quantity required. Together, these changes consistently achieved the target ∼1 mm electrode-to-surface gap and eliminated the delamination and air-cavity defects seen in the earlier iterations. Figure 4.5c shows the finalized mould sample cut in half; the two cavity shapes visible in the cross-section are the imprint of the previously embedded electrodes,the spherical high-voltage electrode at the top and the cylindrical ground electrode at the bottom which were removed after the sample was cut in half.

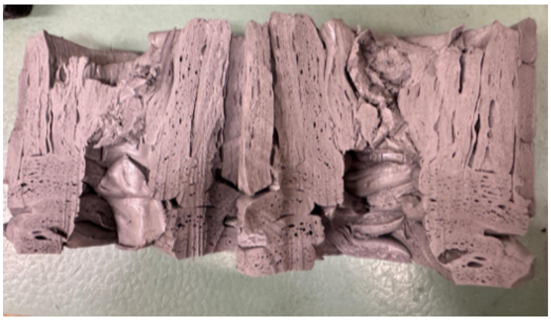

(a) First moulded sample (with cavities)

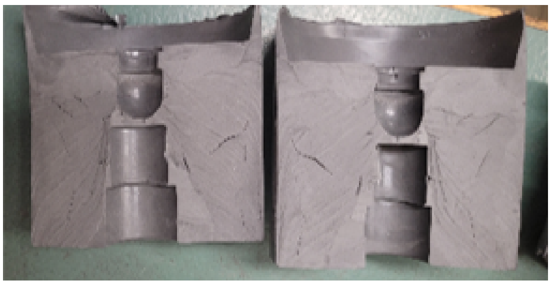

(b) Refined mould sample (with delamination)

(c) Finalised mould sample

Figure 4.5: Solid insulation mould design iterations.

4.4.2 Liquid insulation

The liquid test cell went through a comparable three-stage iterative process before reaching the final test cell design described in 4.3.1.

4.5 Test Standards Compliance

Breakdown testing in this project follows the relevant parts of the **IEC 60243** series, which defines electrode geometry, sample dimensions, and voltage application procedure for electric strength testing of solid insulating materials. **IEC 60243-1** [21] covers testing at power frequency (AC), and is the basis for the mushroom-to-plate electrode geometry used for the AC plate-sample tests (4.2.2); **IEC 60243-2** [23] covers testing using direct voltage, and is the basis for the DC ramp-rate procedure used for both filled EPDM (FGM) and EPDM (4.2.5). Where liquid breakdown testing is intended to characterise the liquid itself as an insulating material, **IEC 60156** (determination of breakdown voltage of insulating liquids at power frequency) is the relevant standard for the electrode geometry and gap distance used.

All other standard-defined parameters – electrode corner radius, surface finish, voltage ramp rate, and the required number of repeated breakdowns were followed exactly as specified in **IEC 60243-1** [21] and **IEC 60243-2** [23]. The gap distances used in this project fall within the ranges permitted by IEC and ASTM for the respective material classes tested, as discussed in 3.3.4; note that for the sphere-to-plate and sphere-to-sphere electrode configurations used here, sample thickness and electrode gap are the same quantity. The sphere-to-plate electrode configuration itself is fully standard-compliant per **IEC 60243-1** [21], and testing with the sample either surrounded by a liquid medium or with the electrodes fully embedded – as used for the half-mould and full-mould configurations – is likewise an option explicitly permitted by the standard, rather than a project-specific deviation.

4.6 Repeatability and Quality Control

Because breakdown is a statistical, weakest-link phenomenon, the reliability of the Weibull analysis in Chapter 5 depends on controlling, as far as practical, every variable other than the one being compared between test series. Several quality-control measures follow directly from the improvement-trial findings in section 4.4:

- Every moulded sample is visually inspected before testing for defects visible at the sample surface and at the electrode interface delamination and deviation from the target ∼1 mm electrode-to-surface gap and samples showing these visible defects are excluded rather than tested. Internal air cavities fully enclosed within the bulk rubber cannot be reliably detected by visual inspection alone; this inspection step therefore reduces, but does not eliminate, the risk of testing a sample with an internal defect, and its main effect is to catch the specific surface and interface-level defects identified during the improvement trials, rather than to guarantee a fully void-free sample.

- Test liquids are visually inspected for trapped air bubbles before each test 4.3.4, for the same reason: a bubble present at the moment of testing is a known, avoidable source of premature breakdown 2.4.3 that would otherwise appear as an unexplained low-strength outlier in the dataset.

4.7 Environmental Test Conditions

Both liquid and solid dielectric behaviour are temperature–dependent (2.2.2, 2.2.4), and the ambient conditions under which breakdown testing is performed can influence the measured results independently of the material or electrode configuration. For this reason, all tests in this work were carried out under controlled laboratory conditions in accordance with the requirements stated in **IEC 60156** [19], **IEC 60243-1** [21]and **IEC 60243-2** [23].

For liquid breakdown testing, the temperature of the insulating liquid was at a range consistent with the environmental recommendations of **IEC 60156** [19], including prevention of bubble formation, ensuring of clean electrode surfaces, and maintaining a stable ambient environment. Solid insulation tests were performed under the same laboratory ambient conditions, following the reference conditions described in **IEC 60243-1** [21] and **IEC 60243-2** [23], where no active heating or cooling is applied unless explicitly required.

Specific temperature and humidity values were not measured or logged throughout the experimental tests; testing instead relied on the laboratory's standard, climate-controlled operating conditions remaining consistent between sessions. This is a limitation of the present methodology: without logged environmental data, small variations in ambient temperature or humidity cannot be ruled out as a contributing factor to the observed scatter in breakdown results, and this could be addressed in future work by recording temperature and humidity alongside each test.

4.8 Safety Considerations

All breakdown testing in this project involves voltages up to 100 kV, requiring standard high-voltage laboratory safety measures throughout. The core hazard is direct or indirect contact with an energised conductor or with a component that remains charged after the supply has been switched off, since a charged capacitance (the test cell, associated cabling, and, for the liquid cell, the dielectric liquid itself) can retain a dangerous stored charge for some time after the voltage source is disconnected.

Consistent with standard high-voltage laboratory practice, testing in this project is carried out inside a locked, protective high-voltage safety cage that prevents operator access to the test cell while voltage is applied. The cage is equipped with a three-state indicator system (green-amber-red) signalling when the area is safe to enter, and is interlocked to the voltage source so that the source is fully disabled and the enclosure can only be opened once the interlock release button is activated. After each test, and before any physical interaction with the setup or the enclosure is opened, the high-voltage and grounded arms of the test cell and associated cabling are manually discharged and earthed using an approved discharge rod, to remove any residual stored charge, whether or not breakdown occurred during that particular test. This procedure, together with the mandatory exclusion zone, ensures that all tests comply with the institutional safety requirements associated with high-voltage laboratories and the operational practices recommended in **IEC 60156** [19], **IEC 60243-1** [21] and **IEC 60243-2** [23].

5

Results

This chapter presents the experimental and simulation results obtained for both solid and liquid insulation materials. The structure follows directly from the test setups, material descriptions, and simulation methodology established in Chapters 1-4. All results are interpreted with respect to the physical mechanisms introduced earlier, and the quality-control measures described in the previous chapters.

5.1 Solid Insulation Results

5.1.1 Electric-Field Distribution in Plate, Half-Mould, and Full-Mould Samples

FEM simulations using COMSOL were performed for the three solid-insulation geometries defined in Section 3.2.3: plate, half-mould, and full-mould. The objective was to quantify the electric-field distribution and identify the location of maximum field stress. To compare the different electrode configurations an exemplary test condition is simulated with a gap distance of 1 mm and a voltage of 10 kV applied between the electrodes for the filled EPDM (FGM), and 80 kV for the unfilled EPDM. The results for the FGM are shown in figure 5.1. It is clearly visible that the plate geometry exhibits extreme field enhancement at the triple point due to the sharp conductivity mismatch between FGM and silicone oil. This results in maximum field greater than 25 kV/mm at the oil-solid-electrode junction. In contrast, the half-mould and full-mould geometries suppress this enhancement by embedding the electrode and replacing the oil region with solid insulation. Their maximum fields are as expected approximately 10 kV/mm, confirming the strong influence of electrode embedding.

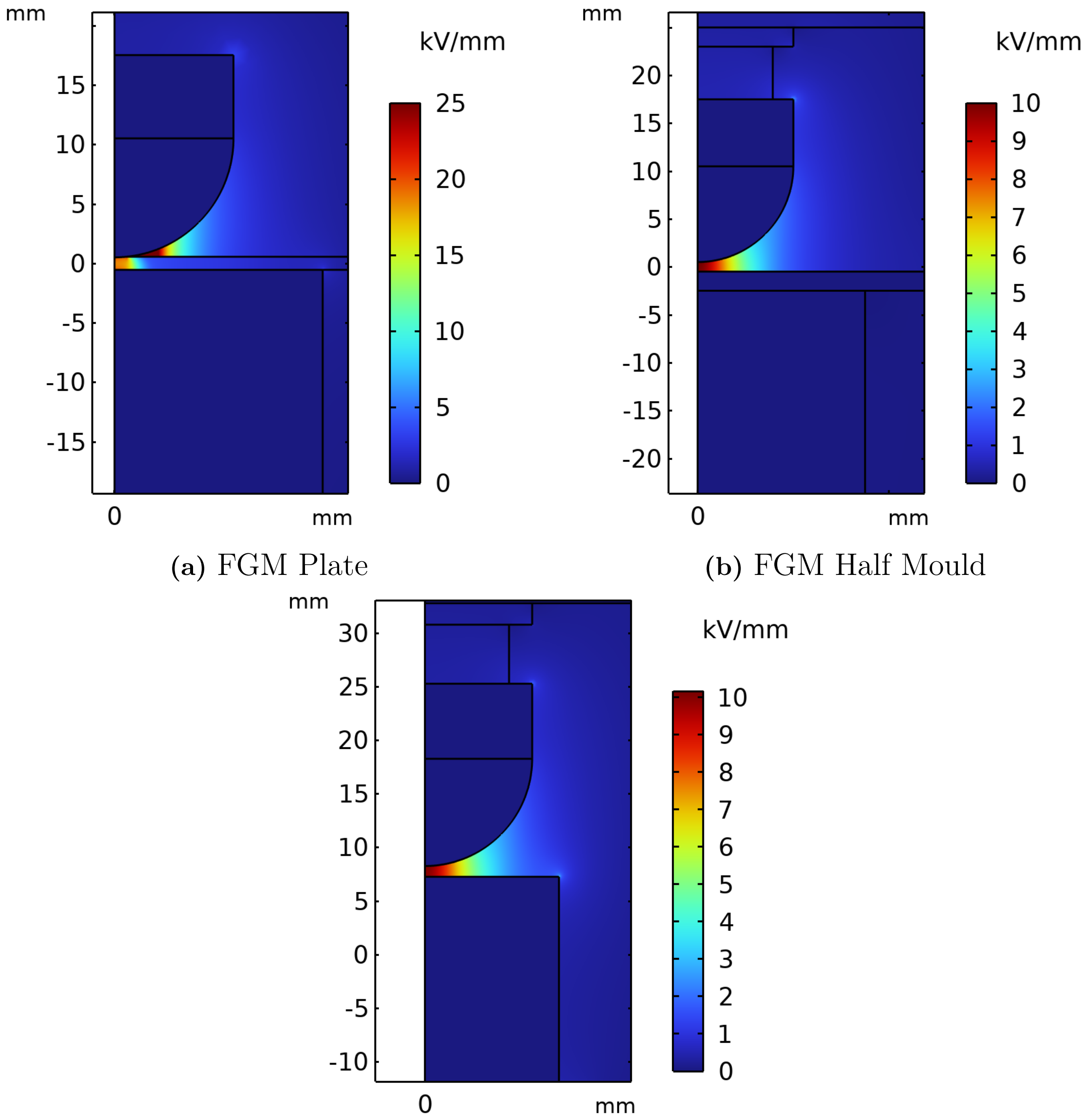

(a) FGM Plate

(b) FGM Half Mould

(c) FGM Full Mould

Figure 5.1: Comparison of electric field strength for the plate, half and full moulded FGM samples.

For the unfilled EPDM the simulation results are shown in figure 5.2. In contrast to the FGM, the plate sample configuration for the unfilled EPDM shows no field enhancement in the oil-solid-electrode junction and the highest electric stress is only inside the solid material. These results confirm the theoretical expectations from Section 2.2.2: materials with high permittivity and nonlinear conductivity such as filled EPDM (FGM) exhibit strong geometry dependence, while the surrounding silicone oil and unfilled EPDM, whose permittivities are closely matched, do not.

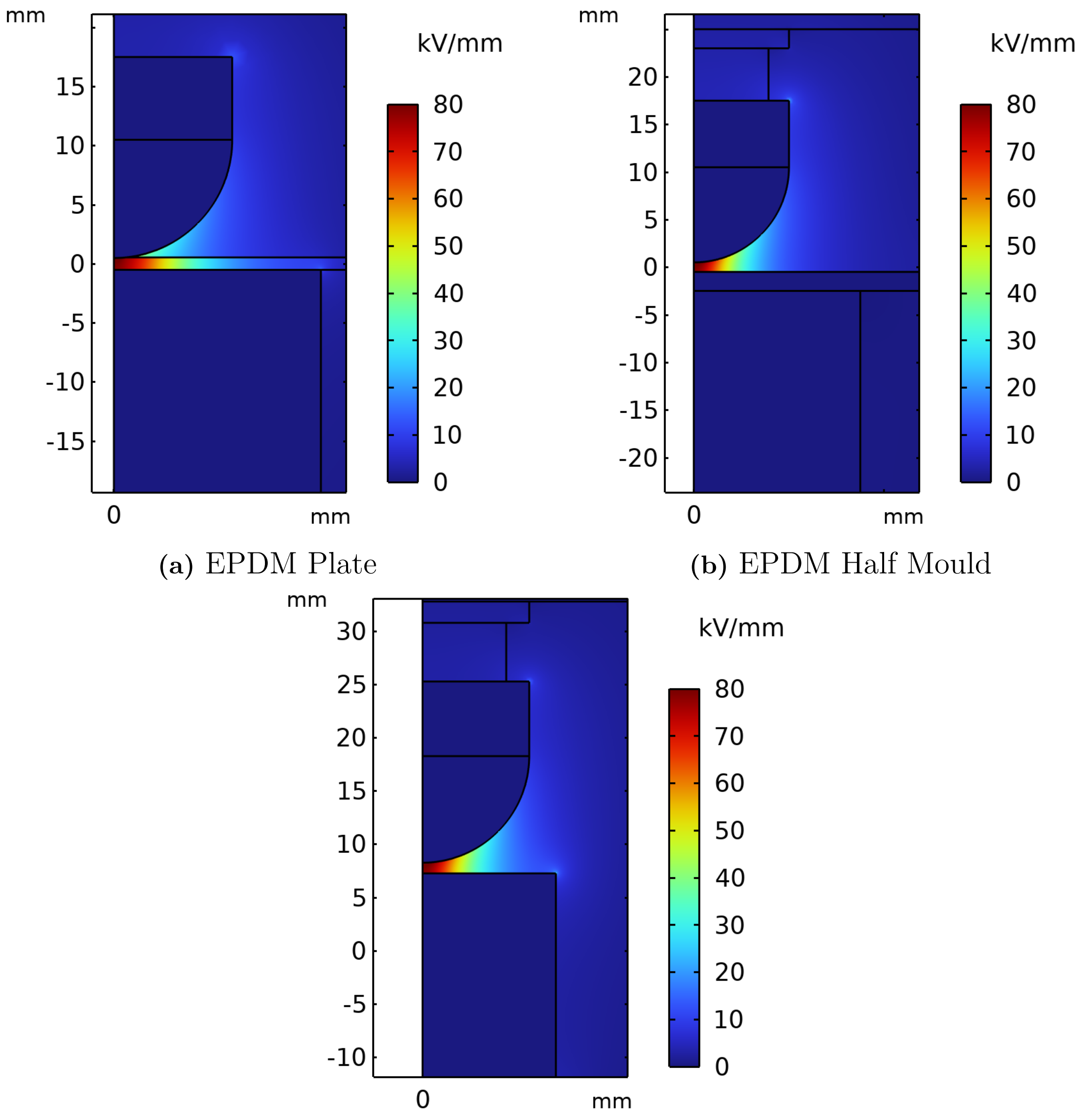

(a) EPDM Plate

(b) EPDM Half Mould

(c) EPDM Full Mould

Figure 5.2: Comparison of electric field strength for the plate, half and full moulded EPDM samples.

5.1.2 Breakdown Strength of FGM and EPDM Across Geometries

Breakdown tests were performed using the procedures defined in Section 4.2. The measured breakdown strengths as seen in figure 5.3 below show a clear contrast between FGM and EPDM.

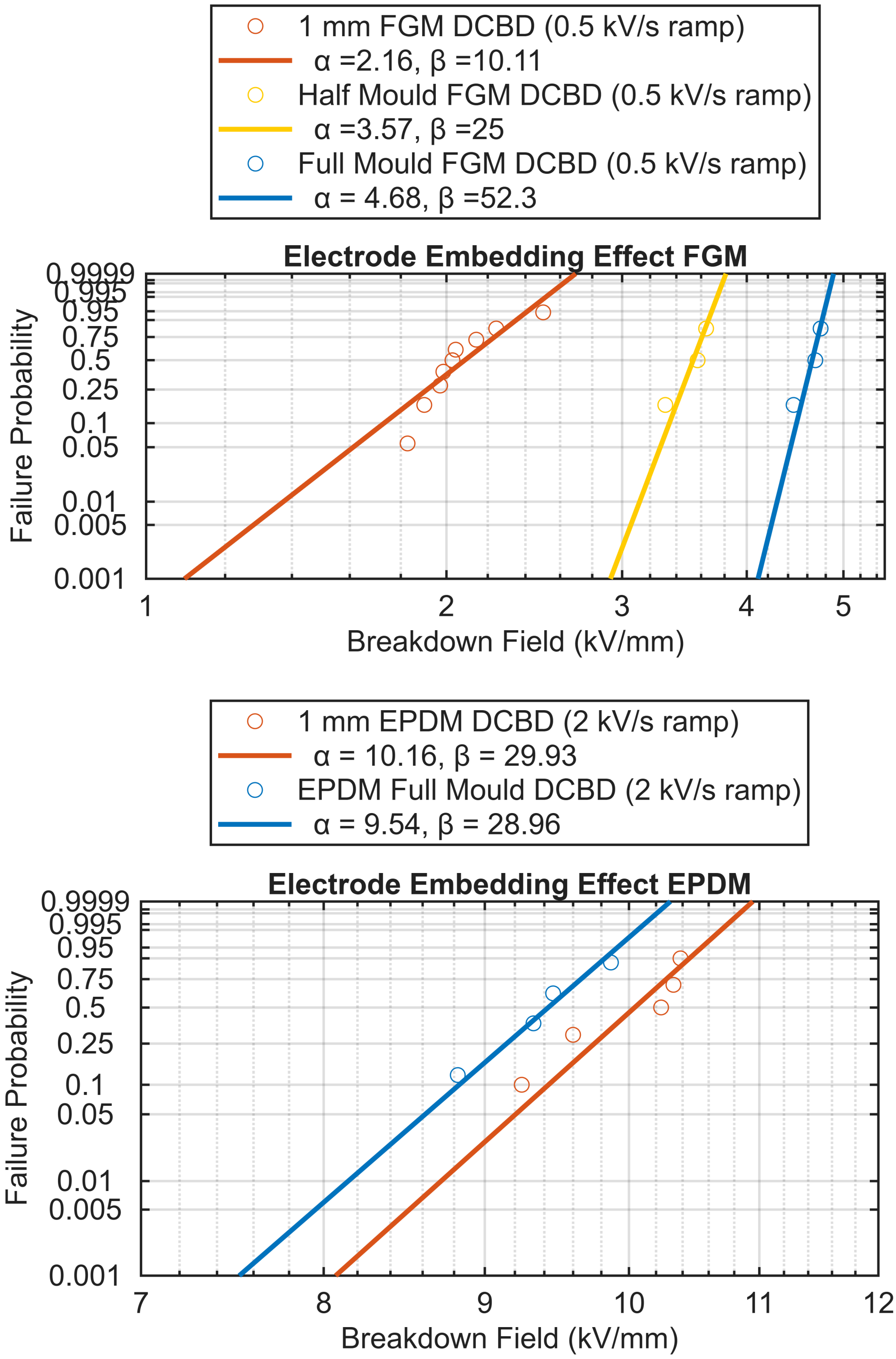

Figure 5.3: Effect of Electrode Embedding on Breakdown Strength: Comparison of Plate, Half-Mould and Full-Mould Configurations

All the mentioned values are normalised measured data, using the same normalisation factor throughout. **FGM:**

- Plate: ∼2.16 kV/mm

- Full-mould: ∼4.68 kV/mm

EPDM:

- Plate: ∼10.16 kV/mm
- Full-mould: ∼9.54 kV/mm

FGM shows a strong dependence on electrode embedding, consistent with the field simulations. EPDM shows only minor variation, confirming the theoretical predictions from Chapter 2.

5.1.3 Thermal Behaviour During DC Stress

Temperature evolution was monitored during DC testing using the setup described in Section 4.2. FGM exhibited a rapid temperature rise due to nonlinear conductivity and Joule heating, eventually reaching thermal runaway. EPDM remained near ambient temperature throughout the test.

The COMSOL simulations results shown in figure 5.4 confirm this behaviour: although filled EPDM (FGM) shows field enhancement at the triple point, this enhanced field occurs predominantly in the surrounding oil rather than in the FGM itself, since the field is pushed out of the more conductive FGM into the adjacent, insulating oil; as a result, the triple-point field enhancement does not translate into additional local heating there. Instead, the significant self-heating observed in FGM originates from the nonlinear conduction current in the bulk material between the two electrodes, where conductivity increases sharply with both field and temperature. EPDM, with its low and weakly temperature-dependent conductivity, shows minimal heating and a stable field distribution throughout.

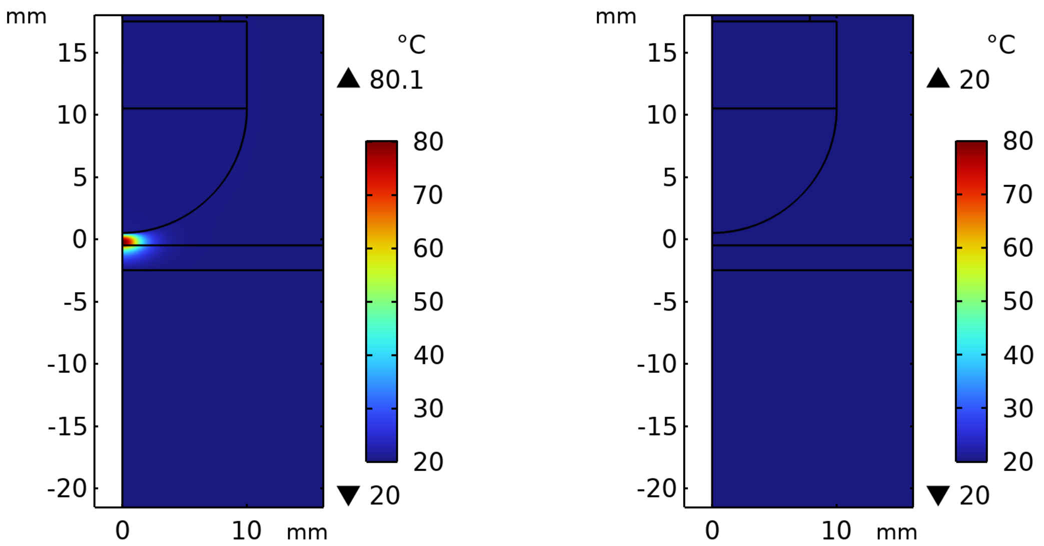

(a) FGM Temperature (b) EPDM Temperature

Figure 5.4: Comparison of temperature between the half mould FGM and EPDM samples.

These results directly support the theoretical model of conduction-driven thermal instability described in Section 2.2.2.

5.2 Liquid Insulation Results

5.2.1 Electric-Field Distribution in the Finalized Test Cell

The finalized liquid test cell was simulated under a 0.5 kV/s DC ramp as seen in figure 5.5 below. Taking the nominal electrode gap of $d = 1$ mm and an applied voltage of $V = 20$ kV as a representative example, the mean (nominal) field is $E_0 = V/d = 20$ kV/mm. The simulated maximum field in silicone oil at this voltage was $E_{\max} = 20.7$ kV/mm, giving a Schwaiger factor of $\eta = E_0/E_{\max} = 20/20.7 \approx 0.966$, confirming a near-homogeneous field distribution.

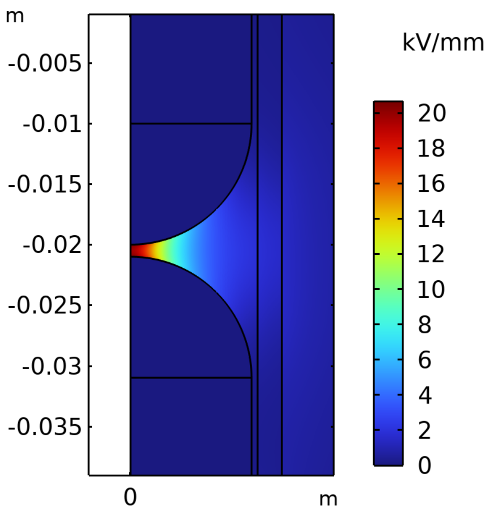

Figure 5.5: Electric field strength - Liquid test cell

5.2.2 Breakdown Strength of Silicone Oil and Silicone Grease

Breakdown tests were performed according to Section 4.3.5. The measured strengths are depicted in the following weibull distribution:

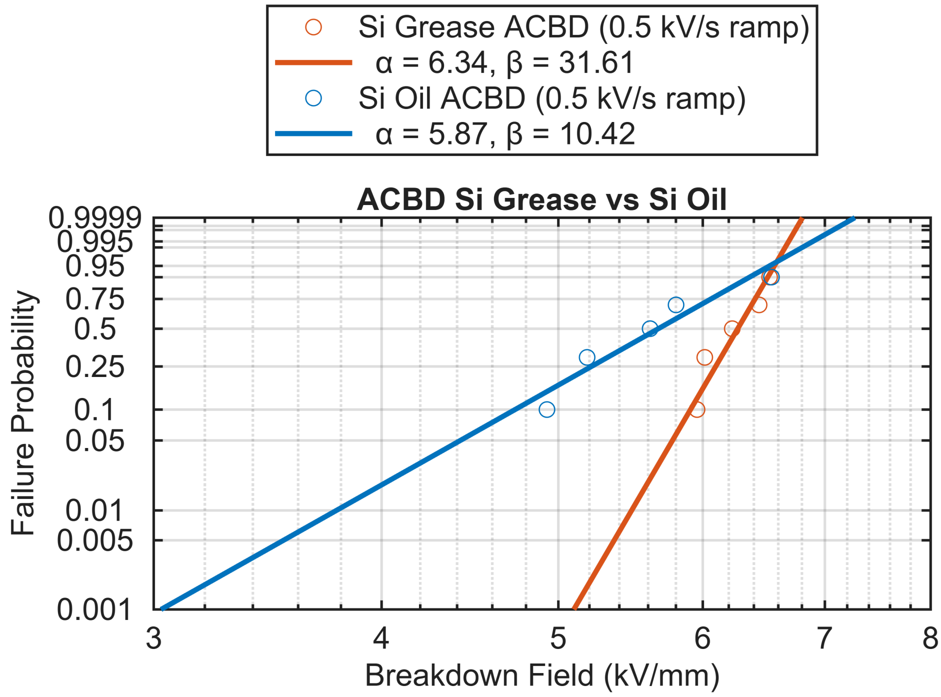

(a) AC Breakdown

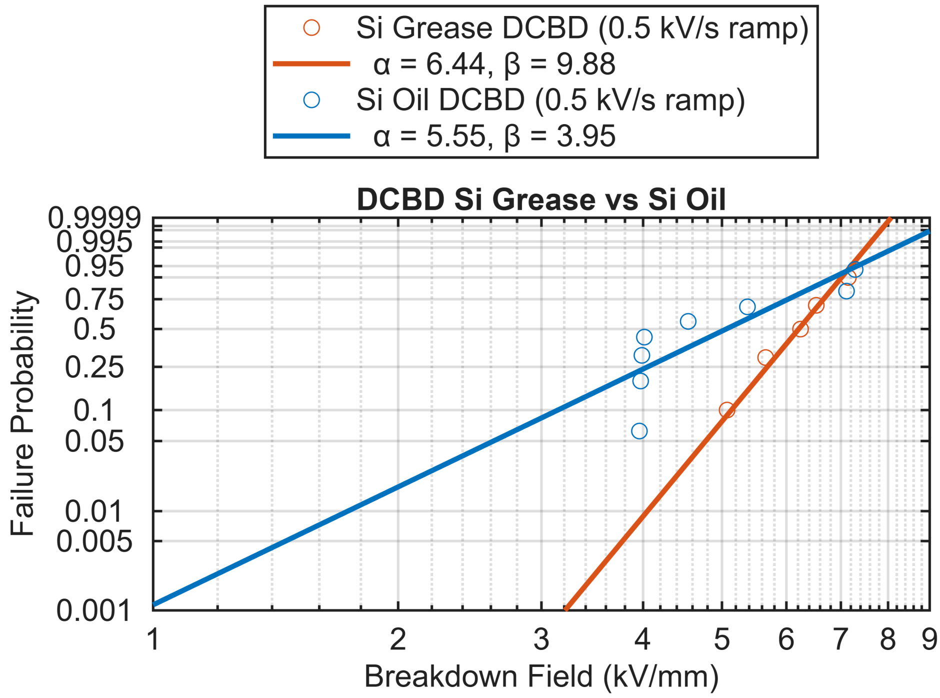

(b) DC Breakdown

Figure 5.6: Weibull probability plots comparing the breakdown field distributions of silicone grease and silicone oil under (a) AC breakdown and (b) DC breakdown test conditions.

Breakdown tests were performed according to 4.3.5. Under AC excitation, silicone grease reached a characteristic breakdown field of $\alpha \approx 6.34$ kV/mm, compared with $\alpha \approx 5.87$ kV/mm for silicone oil. Under DC excitation the same trend held, with grease reaching $\alpha \approx 6.44$ kV/mm against $\alpha \approx 5.55$ kV/mm for oil. Grease outperformed oil under both excitation types, with less scatter, reflected in a consistently higher Weibull shape parameter β.

This may initially seem counter-intuitive, since Stokes' law predicts that a bubble's rise velocity is inversely proportional to viscosity ($v \propto 1/\eta$), meaning grease should in fact be harder to degas than oil, not easier. The higher breakdown strength of grease is therefore unlikely to result from fewer bubbles being present after sample preparation. A more likely explanation is reduced bubble mobility; once loaded, bubbles in the highly viscous grease are less able to migrate into the high-field electrode gap or coalesce into larger, more strongly field-enhancing defects 2.4.3, and any discharge that does initiate faces greater resistance to channel propagation through the more viscous medium 2.4.4. This distinguishes bubble formation from bubble mobility, and is consistent with both the higher characteristic breakdown field and the narrower scatter observed for grease. Confirming this mechanism directly would require dedicated bubble-visualisation or space-charge measurements, which fall outside the scope of this thesis as discussed in Chapter 7

6

Conclusion

6.1 Summary of Findings

6.1.1 Field distribution is strongly geometry-dependent for FGM, but not for EPDM

The COMSOL simulations presented in 5.1.1 show that the plate geometry produces a maximum field greater than 25 kV/mm at the oil-solid-electrode triple point for FGM, compared with the expected 10 kV/mm for the half and full-mould geometries. This confirms the mechanism discussed in 2.2.2 : because the electrical conductivity of FGM differs from that of the surrounding silicone oil by orders of magnitude, any interface between the two materials, as present in the plate configuration, constitutes a severe field discontinuity. EPDM has a low electrical conductivity, so its field distribution remains capacitive (permittivity-controlled) rather than resistive. Since its relative permittivity is close to that of the surrounding oil, it exhibits no comparable field discontinuity at the interface, and the field remains similarly distributed within the electrode gap.

6.1.2 Breakdown-strength trends follow directly from the field simulations and statistical data

This geometry dependence is reflected directly in the measured breakdown strengths. The characteristic breakdown field (α) of FGM more than doubled between the plate configuration ($\alpha \approx 2.14$ kV/mm, $\beta \approx 10.1$) and the full-mould configuration ($\alpha \approx 4.71$ kV/mm, $\beta \approx 52.3$). The simultaneous increase in both α and β is informative in its own right: it shows that removing the triple point does not merely raise the average breakdown strength but also substantially narrows the scatter in the results, indicating that the plate-sample breakdown behaviour was dominated by the field-enhancement defect at the triple point rather than by the intrinsic strength of the material. EPDM, in contrast, showed only a marginal difference between the plate ($\alpha \approx 10.15$ kV/mm) and full-mould ($\alpha \approx 9.54$ kV/mm) configurations, with comparable shape parameters in both cases ($\beta \approx$ 29–30), consistent with a material whose failure is governed primarily by intrinsic or defect-driven breakdown mechanisms 2.3.1 rather than by an electrode geometry induced field concentration.

6.1.3 FGM and EPDM fail through different physical mechanisms

The thermal simulations and the temperature measurements taken during DC testing show FGM undergoing rapid, spatially concentrated self-heating that develops into thermal runaway, a direct consequence of its field-triggered nonlinear conductivity described in 2.3.4. EPDM remained close to ambient temperature throughout testing, consistent with its low and only weakly field-dependent conductivity. EPDM's failures are therefore better explained by the dielectric breakdown driven by presence defects discussed in sections 2.3.1 and 2.3.5: voids, contaminants, and local imperfections introduced during moulding rather than by thermally driven instability.

6.1.4 The liquid test cell achieves a genuinely near-uniform field

The Schwaiger factor of $\eta \approx 0.966$ (2.957 kV/mm simulated versus 2.857 kV/ mm theoretical (normalised), Eq. (4.2)) confirms that the sphere-to-sphere electrode geometry keeps the field close to homogeneous. As discussed in 2.4.4, this means the measured breakdown voltages for the liquid samples are representative of each liquid's intrinsic streamer-initiation strength, rather than being biased by a field concentration introduced by a sharp or divergent electrode.

6.1.5 Comparison of silicone oil and silicone grease under AC and DC stress

Grease showed a higher characteristic breakdown field than oil under both excitation types ($\alpha \approx 6.34$ kV/mm AC and 6.44 kV/mm DC for grease, versus $\alpha \approx 5.87$ kV/mm AC and 5.55 kV/mm DC for oil). This is consistent with the bubble-driven breakdown mechanism discussed in 2.4.3: the higher viscosity of grease suppresses bubble migration and coalescence at the electrode gap, removing one of the dominant practical causes of premature breakdown and scatter identified for liquid insulation.

6.1.6 Necessity of Iterative Mould and Test-Cell Development

The two failure modes documented in 4.1.1 the first moulded sample, and electrode delamination together with inconsistent gap control in the second are themselves examples of the localised field-enhancing defects discussed in 2.3.5. Their elimination through the addition of flow-control grooves in the finalized mould design was a precondition for the full-mould results being interpretable as a genuine measure of intrinsic material strength, rather than as a measurement dominated by manufacturing defects.

6.1.7 Practical implication for cable accessory design

Because the breakdown behaviour of FGM is so strongly dependent on electrode geometry and material interfaces, its performance in a real accessory cannot be reliably inferred from a plate-type, liquid-immersed material test alone; it must instead be tested in either the half-mould or full-mould configuration, so that the results are not impacted by the triple point. EPDM's comparative insensitivity to electrode geometry means that simpler, liquid-immersed test geometries remain an acceptable and more practical choice for characterising its intrinsic breakdown strength.

7

Future Work

While the test setups developed in this thesis successfully characterise the short-time breakdown strength of unfilled EPDM, FGM, silicone oil, and silicone grease, several aspects of insulation performance relevant to cable accessories remain outside the present scope. The following directions are proposed to extend this work.

7.0.1 Long-duration endurance and ageing studies

This thesis explicitly scopes out electrical treeing 2.3.2 and long-term ageing 2.3.6: all breakdown results reported here are short-time tests on the order of seconds to minutes, and cannot capture failure mechanisms that only develop over thousands of voltage cycles or extended DC exposure periods. A natural next step is endurance testing of the finalized full-mould FGM and EPDM samples at field levels below their measured short-time breakdown strength, in order to obtain lifetime versus stress data of the form $t\,E^n \approx$ constant Eq. (2.12), evaluating insulation performance under sustained thermal and electrical ageing rather than a single ramp to breakdown.

7.0.2 Extended material and field-grading profiles

The FGM formulation characterised in this thesis represents a single filler type and loading level 2.3.4. Future work should test additional FGM thicknesses and grading profiles beyond the current sample set, to establish whether the switching-field threshold and the resulting geometry-dependence identified here 5.1.1 generalise across formulations, or are specific to the particular filler system tested in this project.

7.0.3 Higher-voltage validation

The breakdown tests in this thesis were carried out within the operating range of the laboratory equipment (up to 100 kV, Sec. 4.8), using reduced gap distances chosen partly to keep breakdown within this range 3.3.4. Validating the improved test setups both the finalized mould design and the liquid test cell at voltage levels closer to real HVDC service conditions would confirm that the field-uniformity and breakdown-strength trends observed at laboratory scale hold at the higher stress levels the materials actually experience in an installed cable accessory.

7.0.4 Broader liquid dielectric set

The liquid insulation results in this thesis are limited to one silicone oil and one silicone grease formulation 4.1.2. Extending the finalised liquid test cell 4.3.1 to additional dielectric fluids for example alternative lubricant chemistries or oils of differing viscosity would establish whether the viscosity-dependent bubble-suppression mechanism identified for silicone grease 2.4.3 generalises across liquid types, and would broaden the material database available for future cable accessory interface design.

7.0.5 Environmental logging

As noted as a limitation of the present methodology 4.7, temperature and humidity were not logged during testing, and testing instead relied on the laboratory's standard climate-controlled operating conditions remaining consistent between sessions. Future work should instrument the test cage with calibrated temperature and humidity sensors, logging both parameters alongside every breakdown event. This would allow environmental variation to be ruled out as a contributor to the observed Weibull scatter, and would enable a deliberate study of the temperature dependence of the FGM switching threshold itself.

7.0.6 Non-destructive internal defect detection

Section 4.6 notes that visual inspection cannot detect internal air cavities fully enclosed within the bulk rubber, and that the quality-control procedure used in this project therefore reduces, rather than eliminates, the risk of testing a sample with an undetected internal defect. Introducing a non-destructive inspection step for example X-ray tomography, ultrasonic scanning, or dielectric spectroscopy prior to breakdown testing would allow suspect samples to be identified and excluded before testing, tightening the quality control described in 4.6 beyond what surface inspection alone can achieve.

7.0.7 Space-charge and polarity-dependence studies under DC

The theoretical framework in 2.2.3 and 2.2.2 notes that space-charge accumulation and voltage polarity influence the field distribution under DC excitation, but the DC ramp tests carried out in this project do not isolate this effect from the underlying conductivity-controlled field distribution. Follow-up work using polarity-reversal breakdown tests, or direct space-charge measurement techniques such as the pulsed electroacoustic (PEA) method, would help to establish how much of the observed difference between AC and DC breakdown strength for the liquids and for FGM is attributable to space-charge redistribution, as distinct from the conductivity-controlled field split described in 2.2.2.

Bibliography

[1] Kuffel, E., Zaengl, W. S., & Kuffel, J. (2000). *High voltage engineering fundamentals* (2nd ed.). Butterworth-Heinemann.

[2] Eigner, A., & Semino, S. (2013). 50 years of electrical-stress control in cable accessories. *IEEE Electrical Insulation Magazine, 29*(5), 47–55.

[3] Küchler, A. (2018). *High voltage engineering: Fundamentals, technology, applications.* Springer.

[4] Serdyuk, Y. (2008). Electric field distribution in composite insulation systems. *IEEE Transactions on Dielectrics and Electrical Insulation, 15*(1), 52–61.

[5] Yu, H., Liu, Q., & Wang, Z. (2024). Statistical analysis and interpretation on lightning impulse breakdown voltages of ester liquids under varying field uniformity. *High Voltage, 9*(1), 22–34.

[6] Hussain, R., & Andersson, C. (2023). *Electrothermal FEM simulation of relevant test conditions of a 525 kV HVDC cable joint including nonlinear field grading material.* In *Proceedings of the Jicable International Conference on Insulated Power Cables* (Paper A2-2). Lyon, France.

[7] Anghelescu, L., Handra, A. D., & Diaconu, B. M. (2025). Degradation pathways of electrical cable insulation: A review of aging mechanisms and fire hazards. *Fire, 8*(10), Article 397.

[8] Can-Ortiz, A., Laudebat, L., Valdez-Nava, Z., & Diaham, S. (2021). Nonlinear electrical conduction in polymer composites for field grading in high-voltage applications: A review. *Polymers, 13*(9), Article 1370.

[9] Christen, T., Donzel, L., & Greuter, F. (2010). Nonlinear resistive electric field grading part 1: Theory and simulation. *IEEE Electrical Insulation Magazine, 26*(6), 47–59.

[10] Huo, C., Zhuang, J., et al. (2016). Formation mechanism of streamer discharges in liquids: A review. *High Voltage.*

[11] Weibull, W. (1951). A statistical distribution function of wide applicability. *Journal of Applied Mechanics, 18*(3), 293–297.

[12] Feilat, E. A. (2018). Lifetime assessment of electrical insulation. In *Electric field*. IntechOpen. https://doi.org/10.5772/intechopen.72423

[13] Stone, G. C., & Lawless, J. F. (1979). The application of Weibull statistics to insulation aging tests. *IEEE Transactions on Electrical Insulation, EI-14*(5), 233–239.

[14] Bartnikas, R., & Eichhorn, R. M. (1983). *Engineering dielectrics volume I: Corona measurement and interpretation*. ASTM.

[15] Selvasekar, N. S. (2024). *Development and implementation of test cells to perform DC and LI breakdown testing of materials used in HVDC cable accessories* [Master's thesis, Chalmers University of Technology].

[16] COMSOL AB. (2023). *Electrostatics module user's guide*. COMSOL Multiphysics.

[17] Dissado, L. A., & Fleming, R. M. (1996). *Electrical degradation and breakdown in polymers*. Peter Peregrinus Ltd.

[18] Nelson, J. K. (2003). Dielectric polymer nanocomposites. *Journal of Physics D: Applied Physics, 38*, 213–222.

[19] International Electrotechnical Commission. (2018). *Insulating liquids – Determination of the breakdown voltage at power frequency – Test method* (IEC 60156:2018).

[20] ASTM International. (2019). *Standard test method for dielectric breakdown voltage of insulating liquids using VDE electrodes* (ASTM D1816-12(2019)).

[21] International Electrotechnical Commission. (2013). *Electric strength of insulating materials – Test methods – Part 1: Tests at power frequencies* (IEC 60243-1:2013).

[22] ASTM International. (2020). *Standard test method for dielectric breakdown voltage and dielectric strength of solid electrical insulating materials at commercial power frequencies* (ASTM D149-20).

[23] International Electrotechnical Commission. (2013). *Electric strength of insulating materials – Test methods – Part 2: Additional requirements for tests using direct voltage* (IEC 60243-2:2013).

DEPARTMENT OF ELECTRICAL ENGINEERING
CHALMERS UNIVERSITY OF TECHNOLOGY
Gothenburg, Sweden
www.chalmers.se

CHALMERS
UNIVERSITY OF TECHNOLOGY